Unimolecular decay dynamics of Criegee intermediates: Energy-resolved rates, thermal rates, and their atmospheric impact

Thomas A. Stephenson
Department of Chemistry and Biochemistry
Swarthmore College
Swarthmore, PA 19081-1397

Marsha I. Lester
Department of Chemistry
University of Pennsylvania
Philadelphia, PA   19104-6323

ORCID:

Thomas A. Stephenson	0000-0002-2664-5961
Marsha I. Lester	0000-0003-2367-3497

Abstract

Criegee intermediates are highly reactive and energized species formed in the ozonolysis of alkenes. Understanding their chemistry is critical to a comprehensive accounting of OH production, secondary aerosol formation, and the oxidative capacity of the atmosphere. The overall fate of Criegee intermediates in the atmosphere is determined by the competition between bimolecular and unimolecular processes, so a detailed understanding of unimolecular decay is an important topic in both atmospheric and physical chemistry.

The unimolecular decay dynamics of Criegee intermediates is sensitive to the identity of the substituents and conformation of the molecule. Multiple isomerization pathways are possible, with some structures capable of a 1,4-hydrogen transfer reaction that is especially efficient, and generally competes well with bimolecular reactions. Experimental studies that provide energy-resolved rate constants (k(E)) for the process provide important benchmarks for RRKM calculations that can be extrapolated to thermal rate constants (k(T)) under atmospheric conditions. The comparison of k(E) and k(T) values among a series of homologous Criegee intermediates offers insights into the role of structure, energetics, and tunneling in the unimolecular decay dynamics of these species.

Alternative unimolecular decay pathways also illuminate important aspects of the dynamics of Criegee intermediates. These alternative pathways, generally ring closing mechanisms involving heavy atoms, are less susceptible to tunneling and, depending on barriers, may be slower or faster than hydrogen shift processes. Understanding the interplay between unimolecular and bimolecular chemistry of Criegee intermediates under atmospheric conditions remains an active area of research.

Keywords:

Criegee intermediates
Unimolecular dynamics
RRKM theory
Microcanonical rates
Thermal rates

I. Introduction

Alkenes are an important contributor to the hydrocarbon composition of the atmosphere, with both biogenic and anthropogenic sources. One alkene, isoprene (2-methyl-1,3-butadiene), is the most abundant volatile organic compound in the atmosphere, aside from methane. Biogenic emissions (almost exclusively from plants) of isoprene are estimated to exceed 500 Tg per year, while the biogenic emissions of ethene and propene are significantly smaller (< 20 Tg per year).[1] Monoterpene (α- and β-pinene, limonene, etc.) emissions from natural sources are thought to exceed 90 Tg per year. On the other hand, anthropogenic emissions of isoprene are much smaller than those due to plants, ~ 100 Tg per year, and arise from vehicular exhaust and exhaled breath from humans.[2]

Significant reactive pathways for removal of these alkenes from the atmosphere include reactions with ozone (O_3), hydroxyl radicals (OH) and nitrate radicals (NO_3).[3, 4] Ozonolysis of alkenes is a key reaction in understanding the overall oxidizing capacity of the atmosphere, as it both consumes a key oxidant, and can lead to the production of another, OH. Hydroxyl radical is the most important oxidant in the atmosphere, involved in the decomposition of many key pollutants in the lower atmosphere. Field studies have suggested that the ozonolysis of alkenes is responsible for the production of about a third of the atmospheric OH radicals during the daytime, and is the predominant source of OH radicals at night.[5-10]

The initial steps in the ozonolysis of an alkene are shown in Scheme 1, in which O_3 adds across the double bond to form a primary ozonide (POZ).[11] The POZ is formed with significant excess internal energy, and promptly undergoes bond fissure to form a carbonyl oxide compound (the Criegee intermediate) and a carbonyl co-product.[11] Criegee intermediates are formed with significant internal energy and are found to meet

Scheme 1: Alkene ozonolysis proceeds via a primary ozonide, leading to a Criegee intermediate (R_1, R_2) with zwitterionic carbonyl oxide character and carbonyl co-product (R_3, R_4).

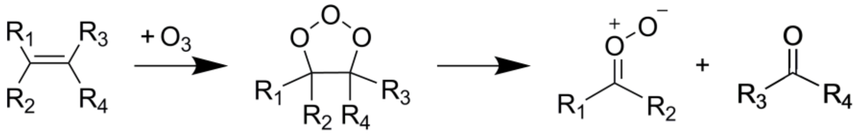

several possible fates under atmospheric conditions: unimolecular decay, stabilization by collisions with non-reactive atmospheric gases (e.g., N_2), or reaction with trace species in the atmosphere (e.g., water vapor, SO_2). Prompt, energized unimolecular decay of Criegee intermediates can lead to the rapid formation of OH and other products, while stabilized Criegee intermediates can undergo thermal unimolecular decay to form OH.[12-15] Stabilized Criegee intermediates can participate in a range of bimolecular reactions, including with water monomers, water dimers, SO_2, carboxylic acids, and alcohols.[16-30] For example, reactive events with SO_2, leading to SO_3, are key to nucleation processes and aerosol formation.[16] Adducts produced in the reaction of Criegee intermediates and carboxylic acids are found to have low volatility and may lead to the formation of secondary organic aerosols under atmospheric conditions.[31-33]

The simplest alkene, ethene (with H substituents at R_1, R_2, R_3, and R_4), undergoes ozonolysis and subsequently forms the Criegee intermediate formaldehyde oxide, CH_2OO, and formaldehyde, CH_2O. This unsubstituted Criegee, once stabilized under atmospheric conditions, can rearrange unimolecularly (to dioxirane) only via a pathway with a high activation barrier (19.1 kcal mol^{-1}).[34] Under atmospheric conditions, the most likely means of removal of this species is reaction with trace gases such as SO_2, NO_2, carboxylic acids, water,[33, 35] and especially water dimer.[22, 23, 36] The slow unimolecular dynamics of stabilized CH_2OO is not believed to substantially contribute to OH production.[37]

On the other hand, ozonolysis of internal alkenes leads to alkyl-substituted Criegee intermediates. For example, the reaction of trans-2-butene with ozone produces a POZ that decomposes to produce the Criegee intermediate acetaldehyde oxide (CH_3CHOO) and acetaldehyde (CH_3CHO).[38] As discussed in section II, one conformer of this Criegee intermediate is capable of following a unimolecular decay path that is fast, leads to efficient production of OH, and competes with bimolecular reactions under atmospheric conditions.

The structure, reactivity and spectroscopy of Criegee intermediates have been the subject of several reviews in recent years.[9, 10, 35, 39-43] For example, Lester and Klippenstein reviewed the numerous studies of the spectroscopy and dynamics of the $(CH_3)_2COO$ Criegee intermediate, focusing on the interplay between experiment and the theory of unimolecular decay.[43] Taatjes *et al.* reviewed the centrality of the bimolecular chemistry of Criegee intermediates to the atmosphere, focusing on the insights gained from laboratory studies.[9] Khan *et al.* considered the bimolecular reactions of thermally stabilized Criegee intermediates, with a particular focus on reactions with water monomers, water dimers, SO_2, and other species that can lead to nucleation in the troposphere.[10] More recently, Taatjes considered the reactivity of Criegee intermediates comprehensively, noting the importance of both energized and stabilized intermediates in the atmosphere, and the challenges that both pose to theory.[41] Shallcross *et al*. have summarized a number of laboratory studies of unimolecular and bimolecular reactions, with the goal of developing insights into the role of stabilized Criegee intermediates in the overall oxidizing capacity of the atmosphere and nucleation processes.[35] Our current effort extends these initiatives by considering the important connection between microcanonical and thermal unimolecular rate constants, the competition with bimolecular reactivity, and their atmospheric impact.

Gaining both an experimental and theoretical understanding of the unimolecular decay of Criegee intermediates under chemically activated and thermalized conditions is critical to assessing the overall impact of these species in the atmosphere. It is also crucial to document how this decay as well as the competition that exists between unimolecular reactions of the Criegee intermediates, stabilizing energy transfer collisions with non-reactive gases, and bimolecular reactive encounters depend on substituents (i.e., the identity of R_1, R_2 in Scheme 1) and their conformation.[44] In section II below, we present the results of a series of experimental studies of the unimolecular rates of decay of Criegee intermediates that are subject to a particularly facile mechanism for the formation of OH: unimolecular 1,4-hydrogen transfer. These experiments are carried out in jet-cooled and collision-free conditions, and with laser preparation of energy-selected states of the reacting molecules. The measured kinetic quantities are thus k(E), the microcanonical rate constant, appropriate for an ensemble in which the energy is well-defined.

In the context of atmospheric chemistry models and experiments, however, the most relevant kinetic quantities are defined in terms of a canonical ensemble, one characterized by a specified temperature, T, rather than a specific energy, E. The more relevant rate constant is thus k(T), the canonical rate constant, rather than k(E). In the absence of quantum mechanical effects such as tunneling, the connections between these two kinetic quantities can be written as,[45]

$$k(T) = \int_{E_0}^{\infty} P(E,T)k(E)dE \tag{1}$$

Here E_0 is the activation energy and $P(E,T)$ is the distribution of internal energies at the temperature T. Gaining an understanding of the thermal, canonical rate constants requires experimental measurements of k(E), and preferably a detailed energy dependence of k(E) so that the integration to determine the thermal rate constant can be carried out with accuracy. Fortunately, theoretical approaches to the calculation of k(E) are available. Direct experimental measurements of k(E) represent invaluable validation of these theoretical approaches and constrain their applicability. This interplay, and the impact on thermal rate constants, k(T), will be a focus of this article.

Statistical Rice-Ramsperger-Kassel-Marcus (RRKM) theory,[45] when informed by high level electronic structure theory, has been shown to be a powerful tool to explore the dynamics of unimolecular decay. The case of Criegee intermediates prepared with well-defined amounts of vibrational energy presents an excellent opportunity to explore the fundamental assumption that sustains the RRKM theory of unimolecular decay: that the molecule, once prepared with an energy E, populates all of phase space statistically, and maintains a uniform phase space distribution during the decay. This will occur if the redistribution of energy among vibrational modes (intramolecular vibrational energy redistribution (IVR)) is rapid compared to reaction, and assures that a microcanonical ensemble, described by the energy E, is maintained throughout the decay. Deviations from RRKM behavior include unimolecular decay rates that differ significantly from the predictions of the theory, or decays that show a sensitivity to variables other than energy, such as the nature of the vibrational quantum state initially prepared.

Energy dependent RRKM rates are evaluated using the formula,[45]

$$k(E) = \frac{\sigma_{eff}}{\sigma^{\dagger}_{eff}} \frac{G^{\dagger}(E - E_0)}{hN(E)} \qquad (2)$$

where $G^{\dagger}(E\text{-}E_0)$ is the sum of states in the transition state, N(E) is the density of states of the reactant (Criegee intermediate), and h is Planck's constant. The effective symmetry numbers, σ_{eff}, are 1 for the reactant with one plane of symmetry, and 0.5 for the transition state with no symmetry and 2 enantiomers (as is the case for some Criegee intermediates). Calculation of the density of states of the reactant requires knowledge of the vibrational degrees of freedom, ideally with anharmonic couplings.

Treatment of the sum of states for the transition state requires accurate knowledge of the energetics of the transition state (from electronic structure calculations), and the vibrational degrees of freedom at the transition state. In addition, critical to exploring the RRKM dynamics of the molecules at energies near or below the transition state barrier is implementing an adequate model of quantum mechanical tunneling. For the reactions considered here, in which 1,4-hydrogen atom shifts are the principle mode of rearrangement, tunneling is efficient and important, owing to the light mass of the transferred atom. This result is also seen in the relatively large (> 1500*i* cm^{-1}) imaginary frequencies associated with the transition states for the unimolecular reactions. We describe below the sensitivity of the microcanonical rate constants, k(E), to the incorporation of tunneling into the RRKM dynamics, and to the details of the reaction path energetics. These features also impact the thermalized rate constants, k(T), through the energy-averaging process; equation (1) by necessity then includes energies below E_0 to capture the impact of the tunneling dynamics.

II. Experimental studies of the unimolecular decay of Criegee intermediates: H-atom shift reactions

The development in recent years of an efficient synthesis for the production of a variety of Criegee intermediates has opened a number of these species to a range of experimental investigations. In this synthesis,[17, 18] a *gem*-diiodoalkane precursor is photolyzed to generate a monoiodo alky radical, which subsequently reacts with O_2 to form Criegee intermediates. This scheme has been used in flow cell applications to study bimolecular chemistry under thermal conditions[41] and in this laboratory to examine unimolecular dynamics in a collision-free jet environment.[43, 46]

In the typical experiment in this laboratory,[47-53] a diiodoalkene precursor is seeded into a rare gas (typically Ar) carrier gas into which O_2 is also entrained. This gas mixture is pulsed through a 1 mm orifice nozzle into a quartz capillary tube (1 mm in diameter, and 25 mm in length). While in the capillary, the precursor is photolyzed using the cylindrically focused, 248 nm output of a KrF excimer laser. One of the C-I bonds is broken photochemically, forming an iodoalkene radical, which reacts with O_2 to form a Criegee intermediate by displacement of the remaining I atom.[17, 18, 54]

Criegee intermediates formed in this way are collisionally stabilized in the capillary and cooled by the free jet expansion, reaching a rotational temperature of ~10K. Once these molecules reach the collision-free region of the expansion (~1 cm below the end of the capillary) they are excited by tunable infrared radiation, preparing the Criegee intermediate in a specific vibrational level (generally C-H stretching fundamental, combination, or overtone) at an energy below or just above the barrier to unimolecular rearrangement. Figure 1 illustrates the overall energetics of the excitation process for a specific alkyl-substituted Criegee intermediate, *syn*-CH_3CHOO; similar energetics are found for others. For those excited Criegee intermediates such as *syn*-CH_3CHOO that can rearrange via a 1,4-hydrogen shift mechanism, this process is greatly enhanced by tunneling through the reaction barrier,[43, 46, 55-59] forming a vinyl hydrogen peroxide (VHP). VHP species are formed with sufficient excess energy to promptly dissociate to form a vinoxy radical and OH. We detect the latter using the intense and well-documented laser-induced fluorescence spectrum. Several distinct studies are possible. First, the OH detection laser wavelength is fixed, and the IR wavelength is scanned, producing an IR action spectrum that mimics the IR absorption spectrum theoretically predicted for the Criegee intermediate.[49, 50, 55-59] For *syn*-CH_3CHOO, the vibrational characteristics of the state(s) excited by the infrared laser are well-understood.[49, 55, 59] Second, the IR laser wavelength is fixed and the OH detection laser is scanned to determine the quantum state distribution of the OH X $^2\Pi$ (v=0) radicals formed in the unimolecular decay,[49, 59] along with the kinetic energy released to the OH and vinoxy radical products in complementary velocity map imaging experiments.[60, 61] But most importantly for this review, both laser wavelengths can be fixed, and the time delay between them scanned, producing a temporal profile for the appearance of the OH products from the unimolecular decay of the Criegee intermediate prepared at specific energies.[43, 46, 55-59] This provides real time microcanonical rate information about the decay of the intermediates.

In Table 1, we summarize the energetic information for the family of Criegee intermediates to be discussed in this section. While the most comprehensively studied intermediate has been *syn*-CH_3CHOO,[46, 49, 55, 58, 59] several other systems have been the subject of IR excitation, followed by UV detection of the OH decomposition products to measure both the IR spectroscopy and microcanonical rate k(E) information.[46, 50, 56, 57, 62, 63] In Figure 2, we have gathered on a single plot the experimentally determined k(E) values from the Criegee intermediates decaying by 1,4-hydrogen shifts. These data are plotted as a function of IR excitation energy (cm^{-1}). The energy of the computed transition state for each molecule is shown as a vertical dashed line. In Scheme 2, we show the general mechanism for the 1,4-hydrogen shift, including the structure of the transition state.

Scheme 2: Generalized unimolecular decay scheme for *syn*-methyl Criegee intermediates with various substituents R leading to OH radical products

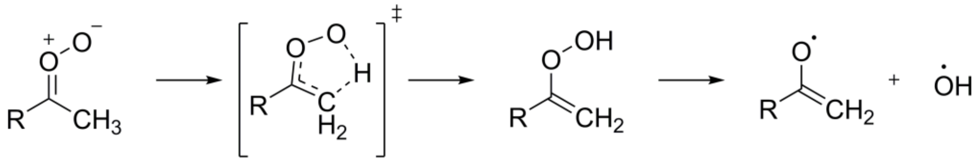

CH3CHOO dynamics

CH_3CHOO is the simplest Criegee intermediate with an alkyl substituent capable of a 1, 4-hydrogen transfer reaction to form a vinyl hydroperoxide. It exists, however, in two conformational forms, referred to as *syn*- and *anti*-, separated by a high barrier arising from internal rotation about the C=O bond. In the less stable *anti*-conformation, (ca. 3.4 kcal mol^{-1} higher in energy than the *syn*-conformation[38, 64-66]) the terminal O atom faces the H atom attached to the $C=O^{+}-O^{-}$ functional group, which mimics the geometry of the unsubstituted Criegee intermediate, CH_2OO, and similarly does not yield significant OH products. In the more stable *syn*-CH_3CHOO, the terminal O atom faces the H atoms of the methyl group, one of which is transferred to form a hydroperoxide.

The unimolecular decay dynamics of *syn*-CH_3CHOO have been examined in three distinct energy regimes, accessed using the C-H first overtone vibrations (5600 – 6100 cm^{-1}), [46] C-H stretch + ν_i combination bands (4100 – 4400 cm^{-1}),[55] and C-H fundamental vibrations (2900 – 3100 cm^{-1}).[59] As shown in Figure 2, near the top of the activation barrier (5963 cm^{-1}; 17.05 kcal mol^{-1}), this Criegee intermediate decays with the fastest rate observed of this class of compounds, with an OH product rise time of ~5 ns (k(E) ~ 2 X 10^8 s^{-1}), within the experimental temporal resolution.[46] Spectroscopic studies and vibrational perturbation theory calculations confirm that the vibrational features excited in this region are transitions involving two quanta of CH stretch in a single mode (e.g., $2\nu_1$) or one quantum each in two CH stretch modes (e.g., $\nu_1 + \nu_2$).[49] The vibrational features, while characterized by a rotational temperature of 10K (consistent with the free jet expansion conditions used to stabilize the Criegee intermediate), are observed to be homogeneously broadened. The spectral line broadening is consistent with an intramolecular vibrational energy redistribution (IVR) lifetime in this energy range of ~ 3 ps, and indicates that IVR in IR-activated *syn*-CH_3CHOO is orders of magnitude faster than its unimolecular decay to OH products.[46]

At lower energies (4100 – 4400 cm^{-1}), a smaller degree of homogeneous line broadening is observed, consistent with the smaller overall density of states.[55] An IVR lifetime of ~ 9 ps is assigned based on spectral fitting of the rotational band contour. Comparison with theoretically predicted IR absorption spectra suggests that the vibrations observed in this spectral region are combination bands composed of one quantum of CH stretch and one quantum of one of the following lower frequency modes: CH in-plane wag; CCO backbone bend; methyl umbrella; or methyl asymmetric scissors. As shown in Figure 2, in this energy regime the decay dynamics that yield OH products occur on a timescale that is nearly two orders of magnitude slower than the decay that occurs near the top of the reaction barrier. The OH appearance rise times, 310 – 650 ns, vary monotonically with energy, as expected for a process that is driven by tunneling through the reaction barrier. There are no clear mode specific effects to the dynamics, consistent with a rapid statistical redistribution of energy following the initial vibrational excitation.

Not displayed in Figure 2 are results from experimental measurements performed in the region of the CH fundamental vibrations, 2900 – 3100 cm^{-1}.[59] IR-activated *syn*-CH_3CHOO molecules decay significantly slower than at higher energies. A lower limit of 2 μs was established for the OH appearance time [$k(E) \leq 5 X 10^5 s^{-1}$] following IR excitation of *syn*-CH_3CHOO at ca. 3000 cm^{-1}. Experimental constraints arising from the molecules moving out of the probe region did not permit direct measurement of the slow unimolecular decay rates in this energy region. The low density of vibrational states at these energies (~ 5 states/cm^{-1}) are on the order of the threshold vibrational state density (~10 states/cm^{-1}) required for extensive population relaxation by IVR under jet-cooled conditions.[67, 68] This makes the interpretation of IVR dynamics less straightforward than at higher energies, as there is the possibility of incomplete IVR and mode-specific effects in the unimolecular decay rates. The different CH stretch features observed spectroscopically have varying degrees of homogeneous broadening, an indication of mode-specific coupling that initiates the redistribution process. Nevertheless, the appearance of OH products demonstrates that there is at least some degree of IVR from the initially excited CH stretches to the modes that evolve into the reaction coordinate at these energies.

The importance of tunneling in the unimolecular decay dynamics of *syn*-CH_3CHOO, even at energies near the transition state barrier, is further revealed in experiments on a selectively deuterated Criegee intermediate, *syn*-CD_3CHOO.[58] In these experiments, the first overtone of the CH stretch is excited to provide ~ 6000 cm^{-1} of vibrational energy, as before, but now the atom transferred is a deuterium, to form the VDP species, CD_2=CHOOD, and releasing OD products that are detected. Three possible effects contribute to the impact of deuteration on the values of the microcanonical rates. First, electronic structure calculations show that the isotopic substitution increases the zero-point energy (ZPE) corrected barrier height slightly from 17.05 kcal mol^{-1} (5960 cm^{-1}) for *syn*-CH_3CHOO to 17.74 kcal mol^{-1} (6205 cm^{-1}) for CD_3CHOO. This increase in the barrier height for *syn*-CD_3CHOO results from a larger decrease in ZPE in the reactant than at the transition state upon deuteration. Second, the heavier D atom in the reactant *syn*-CD_3CHOO also result in higher values of the density of states, N(E), at all energies relative to the density of states for *syn*-CH_3CHOO. Third, and most importantly, the transfer of the heavier D atom at the transition state results in a lower imaginary frequency, 1325i cm^{-1}, along the reaction coordinate compared to the fully hydrogenated *syn*-CH_3CHOO (1696i cm^{-1}). The result of all of these factors is a kinetic isotope effect (KIE) on the microcanonical unimolecular decay rate that is smaller (~8) at energies near the top of the activation barrier, and increases (to ~200) at energies ~2000 cm^{-1} below the barrier. Since the ratio of N(E) values for *syn*-CH_3CHOO relative to *syn*-CD_3CHOO is largely energy-independent, the change in KIE with energy reflects the decreased probability of tunneling for the heavier D atom relative to the lighter H atom, a factor that is more significant as the barrier becomes more difficult to penetrate.

While the detection of the infrared action spectrum of the Criegee intermediate requires that the vinyl hydroperoxide molecule produced in the unimolecular decay ultimately yield an OH radical, we note that other outcomes are possible. Specifically, Kuwata *et al.*, have found in theoretical calculations that a roaming transition state is possible, leading to the formation of an internal OH transfer product, hydroxyacetaldehyde.[69] IR action spectroscopy focused on detection of free OH would not be sensitive to this pathway.

$(CH_3)_2COO$ dynamics

Similar studies of the unimolecular decay dynamics of the dimethyl-Criegee intermediate, $(CH_3)_2COO$, have been carried out.[46, 50, 57] Note that for this molecule, there are no conformational complications as in CH_3CHOO because methyl groups occupy both substituent sites on the carbon of the carbonyl oxide. In this case, the substituted VHP $CH_2{=}C(CH_3)OOH$ is produced, which promptly decomposes to yield OH plus the methyl-substituted vinoxy radical $CH_2{=}C(CH_3)O$. As shown in Figure 2, both the CH first overtone and combination bands involving CH stretch and a lower frequency mode, have been investigated. The unimolecular decay kinetics of $(CH_3)_2COO$ are found to be slower than that of CH_3CHOO by a factor of ~4 throughout the energy range. In section III below we review the results of RRKM calculations that have been performed on the unimolecular decay dynamics of these Criegee intermediates. At this point, it suffices to note that the change in the decay rates, while dominated by the increased density of states in $(CH_3)_2COO$, is moderated by the slightly lower barrier (5652 cm^{-1}; 16.16 kcal mol^{-1}) to reaction (and enhanced tunneling) that is observed in this molecule.[46] (We note that $G^{\dagger}(E-E_0)$ changes, too, but by much less than N(E).) The unimolecular decay dynamics of $(CH_3)_2COO$ have been the subject of a recent review.[43]

Similar to *syn*-CH_3CHOO, a roaming transition state for the decay of energized $(CH_3)_2COO$ has been identified by Kuwata, *et al*.[69] In this case, the OH radical is internally transferred to form hydroxyacetone. As in the case discussed earlier, the formation of this product would not be detected in the infrared action spectrum, but has been observed arising from the unimolecular decay of thermalized samples of $(CH_3)_2COO$.[70]

CH_3CH_2CHOO dynamics

Studies of the ethyl-substituted Criegee intermediate are attractive from a number of perspectives.[56] First, unlike the prior cases, the H atom to be transferred is from a secondary carbon (-CH_2-). Second, the terminal methyl group affords additional stabilization to the radical vinoxy product that results from OH production, relative to the isomeric dimethyl Criegee intermediate. Third, the ethyl-substituted molecule is a model for Criegee species with longer alkyl chains which can be formed from reactions from the ozonolysis of long chain alkenes in the troposphere.

In addition to *syn*- and *anti*-conformers, the ethyl (and all longer chain Criegee intermediates) have more complicated conformational dynamics. In this case, rotation about the central C-C bond produces two distinct conformers, both with the *syn*-orientation required for 1,4 - hydrogen transfer. These conformers differ in the value of the dihedral angle τ_{CCCO}, and both are expected to be present in the free jet expansion source.[71] (These conformers are predicted to have very similar IR spectra in the CH overtone region at the experimental resolution.) The experimental measurement of rates, however, revealed that excitation of the slightly higher energy transition (see Figure 2) resulted in a smaller k(E) than the lower energy excitation, counter to the expected energy-dependent trend. The interpretation is that the lower energy transition is preparing the less stable conformer in a higher vibrational state, which results in a ~30% faster unimolecular decay rate. Overall, the decay rates for CH_3CH_2CHOO are slower than those of $(CH_3)_2COO$ by about a factor of 2, despite having the same molecular weight and overall number of degrees of freedom, and a transition state barrier that is only 105 cm^{-1} (0.30 kcal mol^{-1}) higher. The torsional motion, and lower vibrational frequencies associated with the ethyl side chain, however, provide a higher density of states and dominant contribution to the slower unimolecular rate (note that the TS lacks an ethyl rotor), as compared to $(CH_3)_2COO$. We discuss the implications of molecular properties on the RRKM calculations and unimolecular dynamics in greater detail in section III.

Methyl Vinyl Ketone Oxide (MVK-oxide) dynamics

An important sink of tropospheric isoprene (2-methyl-1,3-butadiene) is reaction with ozone (~10%),[72] which yields three possible Criegee intermediates, methyl vinyl ketone oxide (MVK-oxide), methacrolein oxide (MACR-oxide, $CH_2{=}C(CH_3)CHOO$), and CH_2OO as shown in Scheme 3.[72-74] Only one set (*syn*) of MVK-oxide conformers has the requisite structure to undergo a 1,4 – hydrogen shift unimolecular rearrangement to produce a vinyl hydroperoxide and then promptly generate OH.[62] MVK-oxide is also predicted to be the more abundant four carbon unsaturated Criegee intermediate.[72]

Scheme 3: Criegee intermediates and co-products formed in ozonolysis of isoprene.

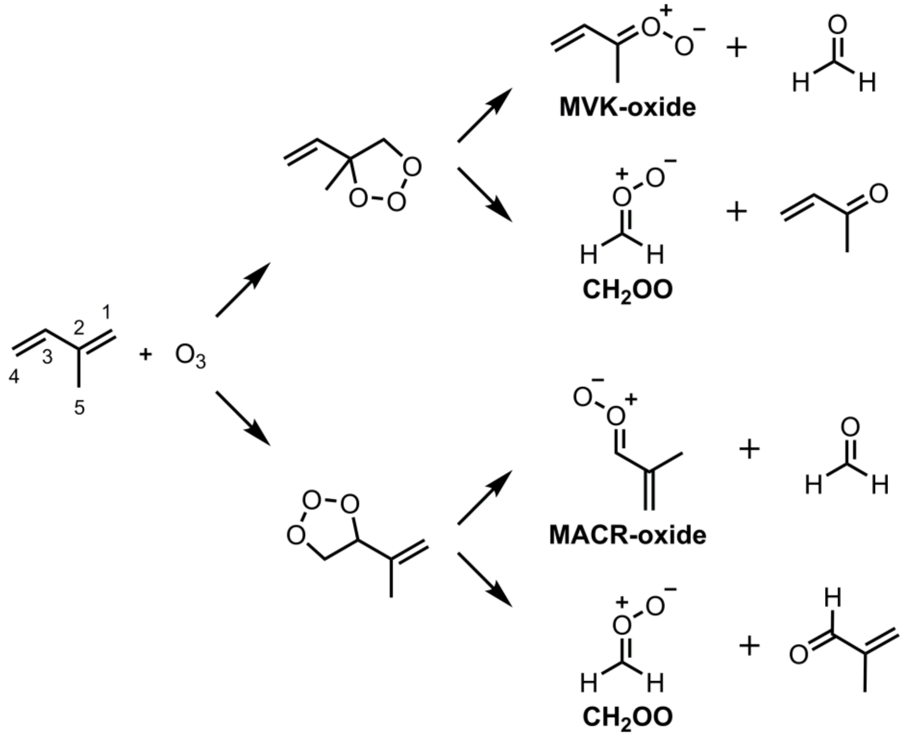

As shown in Figure 3, MVK-oxide is predicted to have four conformers, which differ by the orientation of the methyl group with respect to the terminal oxygen atom (*syn* and *anti*-conformers), and the relative orientation of the C=C and C=O bonds (*cis* and *trans* isomers). High level electronic structure calculations demonstrate that the energies of all four conformers lie within 3.1 kcal mol^{-1} of one another, with the *syn*-*trans* form the most stable.[62, 75] There are, however, substantial barriers to interconversion between the conformers. The *syn*-to-*anti* barrier is calculated to be ~30 kcal mol^{-1}, while the barriers to conversion between *cis* and *trans* forms are ca. 10 kcal mol^{-1}.[44, 62, 75] All four conformers are likely produced in the synthetic scheme and cooled in the free jet expansion, but only the *syn*-conformers are capable of the 1,4 – hydrogen shift reaction, forming the vinyl hydroperoxide (2-hydroperoxybuta-1,3-diene, $(CH_2{=}CH)$-(CH_2)-COOH, HPBD) that dissociates to release OH products. In Scheme 4, the mechanism for the unimolecular decay of *syn-trans*-MVK-oxide to produce OH is shown.

Scheme 4: Unimolecular decay pathway for *syn-trans*-MVK-oxide to OH + oxybutadiene (OBD) radicals.

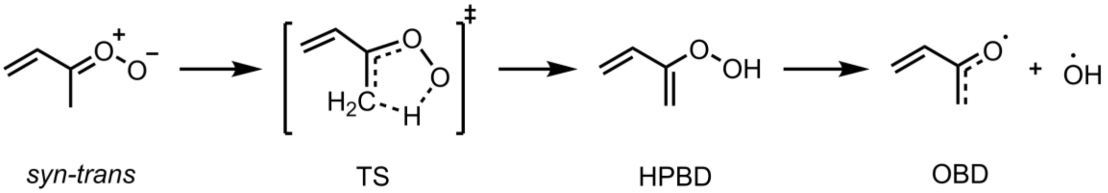

The infrared action spectroscopy of the MVK-oxide is complicated by the presence of multiple conformers and the large number (21) of transitions predicted in the 5750 – 6300 cm^{-1} spectral region: six CH stretch overtones and 15 CH stretch combinations per conformer.[62] Nevertheless, with the aid of computed anharmonic frequencies and IR intensities, assignments were made to features corresponding to both *syn*- and *anti*-conformers. (See section IV for a discussion of the pathways for the decay of vibrationally excited *anti*-MVK-oxide.) The k(E) value securely assigned to the decay of *syn-trans*-MVK-oxide is shown in Figure 2. *Syn-trans*-MVK-oxide is observed to decay at a rate that is ~ 100 times slower than *syn*-CH_3CHOO at comparable amounts of vibrational excitation, a result of the somewhat higher barrier to reaction (see Table 1) and the larger density of states in the first overtone region.

In addition to unimolecular decay that leads to OH radicals, a roaming transition state has been identified for MVK-oxide,[62] as has been predicted in CH_3CHOO and $(CH_3)_2COO$.[69] In this case, the minimum energy path passes over saddle points that are actually lower in energy than the asymptote corresponding to bond fission to form free OH.

It is possible, therefore, that the roaming mechanism is significant in the dynamics of isoprene-derived Criegee intermediates under atmospheric conditions.

III. RRKM calculations of the unimolecular decay of Criegee intermediates: H-atom shift reactions

Microcanonical Rate Constants, k(E)

RRKM theory has been very effective in modeling the dynamics of the unimolecular decay in the Criegee intermediates subject to 1,4-hydrogen transfer. For *syn*-CH_3CHOO, RRKM calculations have been considered at energies corresponding to excitation at the first C-H overtone (~6000 cm^{-1}), C-H stretch + ν_i combination bands (~ 4200 cm^{-1}), and C-H stretch fundamental (~3000 cm^{-1}). Calculations on deuterated analogues of *syn*-CH_3CHOO have been performed as well.

In Figure 2, we plotted the calculated k(E) values derived from RRKM calculations for *syn*-CH_3CHOO over the energy range 4000 – 6300 cm^{-1}, along with the experimentally determined unimolecular decay rates discussed previously.[46, 55] As we have described, critical to implementation of the RRKM theory for unimolecular events near or below the transition state energy is an adequate model for quantum mechanical tunneling. Two models are used for calculating tunneling coefficients, and thus for weighting the transition state sum of states. In the first, a one-dimensional Eckart potential is calculated from the imaginary frequency at the transition state, and the forward and reverse reaction barriers.[76] Energy dependent transmission coefficients can be calculated within this model analytically.[45] Figure 2 shows the calculated k(E) values that are based on the Eckart model for tunneling.[46, 57, 62] The second model of tunneling incorporates semi-classical transition state theory, as formulated by W.H. Miller and co-workers,[77] and implemented in the MULTIWELL suite of programs.[78-80] Other groups including Truhlar and coworkers use the small-curvature tunneling approximation.[66, 81] Very little quantitative difference is found between these approaches to simulating tunneling in the systems investigated thus far; in this review, we use the Eckart approach to illustrate comparative features of the molecular systems because of the ease of visualization.

The agreement between the experimental and theoretical values in Figure 2 is qualitatively excellent, validating in a global sense the assumption of a statistical distribution of energy within the *syn*-CH_3CHOO and the dimethyl-substituted Criegee intermediates.[46, 55, 57] These results also validate the results of the electronic structure calculations which provide the transition state energies, structures, and imaginary frequencies – all critical parameters in the RRKM calculations. It is also possible to calculate RRKM rates in which tunneling is explicitly ignored.[55, 57] In these cases, the calculated rates are zero for energies below the energy of the transition state, and rise abruptly at the transition state energy, trends that are in sharp variance with the experimental results.

A careful examination of Figure 2 reveals that for *syn*-CH_3CHOO at energies between 4000 and 4500 cm^{-1},[55] there are discrepancies between the experimental measurements and the RRKM calculations that are outside the experimental uncertainties (not shown, but are ±1σ based on repeated measurements). Particularly in this lower energy regime, where the density of states is smaller, it is possible that fluctuations in the rates arise from the sparsity of vibrational states available for the redistribution of energy and/or a modest degree of mode selectivity in the unimolecular dynamics. Wagner has proposed improvements to the SCTST treatment that is a more accurate representation of deep tunneling.[82] This modification, however, does not introduce fluctuations over narrow energy regions like that displayed in Figure 2, and thus will not explain these experimental results.

The dynamics of *syn*-CH_3CHOO have been examined at lower energies, in the region of the C-H stretch fundamental vibration (2900 – 3100 cm^{-1}).[59] For the Criegee intermediates prepared with this amount of energy, unimolecular decay occurs at a rate that is too slow ($\geq 2\mu s$) to quantitatively measure using the present setup, so a detailed comparison with RRKM calculations was not possible. Significant variations in the linewidths of spectral features suggest, however, that selective mode-specific couplings are present that may affect the unimolecular dynamics. We expect that the low density of states in this region (~ 5 vibrational states/ cm^{-1} on average) will represent a challenge to underlying assumptions of RRKM theory. A challenge left to future experiments will be to extract quantitative measurements of microcanonical rates to test whether there is a breakdown in the RRKM calculations in the energy regime of the C-H stretch fundamental vibration.

The RRKM calculations provide a means to understand in physical terms the trends observed in the k(E) values upon chemical substitution of the Criegee intermediates. Here we focus exclusively on the microcanonical rates in Figure 2 near or just above the energy of the transition states. We observe the clear trend in the rates of unimolecular decay:

$$CH_3CHOO > (CH_3)_2COO > CH_3CH_2CHOO > \text{MVK-oxide}.$$

Examination of Table 1 demonstrates that this trend is not simply explained by the magnitude of the forward activation barriers. Figure 2 shows that the variation from one molecule to another is large and can be greater than the dependence of the rate on energy for any one molecule.

Within RRKM theory, the rate is determined by two quantities, the density of states in the reactant, N(E), and the sum of states at the transition state, $G^{\dagger}(E\text{-}E_0)$, with the latter quantity appropriately weighted for tunneling.[45] Both play a role in understanding the impact of changing the substituents of the Criegee intermediates. N(E) of the reactant Criegee intermediates increases steadily with molecular complexity, i.e., for N(E) values:

$$\text{MVK-oxide} \gg CH_3CH_2CHOO > (CH_3)_2COO \gg CH_3CHOO.$$

The case that underscores the power of the RRKM calculations in revealing physical details of the reactivity is the comparison of the ethyl- and dimethyl-substituted Criegee intermediates.[46, 56, 57] As shown in Figure 4 the ethyl-substituted Criegee intermediate has a larger density of states at each energy than the dimethyl-substituted Criegee intermediate – molecules with the same molecular weight and number of vibrational degrees of freedom. (For example, at 5900 cm^{-1}, the densities of states differ by a factor of 1.6.) This effect is due to the larger number of torsional states associated with the ethyl rotor (which contains a methyl rotor), relative to the dimethyl-substituted Criegee intermediate, which contains two independent methyl rotors. Although both the ethyl- and dimethyl-substituted Criegee intermediates contain two alkyl rotors, rotation about the secondary ($-CH_2-$) alkyl bond has a much larger effective reduced mass as compared to a methyl rotor. The ethyl-substituted Criegee intermediate is expected, therefore, to have a larger density of torsional states. As also plotted in Figure 4, the trend in the transition state sum of states $G^{\dagger}(E\text{-}E_0)$ is qualitatively different. The sums of states for the ethyl- and dimethyl-substituted Criegee intermediates are very similar, with the ethyl-substituted

Criegee intermediate value of G†(E-E$_0$) larger by a factor of only 1.04. This similarity is due to the geometry of the transition state. As shown in Scheme 5, in the ethyl-substituted Criegee intermediate, the secondary carbon of the ethyl rotor is incorporated into 1,4-hydrogen atom transfer five membered ring, reducing its conformational flexibility. Only the terminal methyl rotor remains relatively unhindered.

Scheme 5: Unimolecular decay pathway for ethyl-substituted Criegee intermediate to OH products. Note the loss of internal rotation about the secondary (-CH$_2$-) alkyl bond at the transition state, leaving a single methyl rotor.

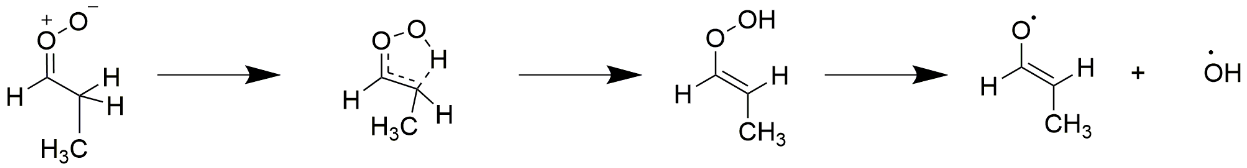

In the dimethyl-substituted Criegee intermediate, one of the methyl rotors is incorporated into the 1,4-hydrogen atom transfer transition state, leaving a single methyl rotor unhindered, just as in the ethyl-substituted Criegee intermediate transition state (see Scheme 6).

Scheme 6: Unimolecular decay pathway for dimethyl-substituted Criegee intermediate to OH products. Note the loss of one of two methyl rotors at the transition state.

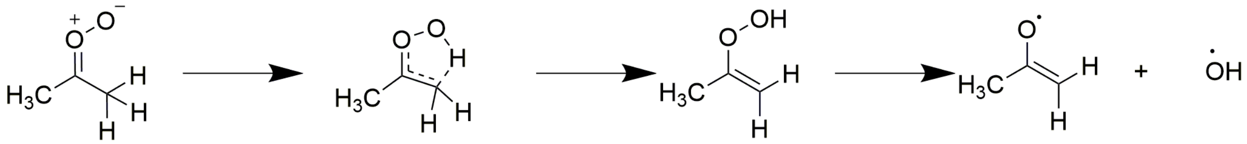

Thus, unlike the reactants, the transition state structures have similar methyl torsional characteristics. The ratio of the sum of states G†(E-E$_0$) to the density of states N(E), which determines the microcanonical rate constant, is therefore reduced for the ethyl-substituted Criegee intermediate.

Overall, the variation in the microcanonical rates for the Criegee intermediates displayed in Figure 2 is dominated by the changes in the densities of reactant states. The barriers to reaction vary from 16 to 18 kcal mol^{-1} (see Table 1), depending on the substituents,[63] and the imaginary frequencies along the reaction coordinates change by a similar degree, as revealed in Figure 5. Here we plot the Eckart potentials used in RRKM calculations to model quantum mechanical tunneling in these systems. More careful examination reveals, however, that there are factors that moderate (or enhance) the rates of decomposition other than the densities of states. For example, the enhanced rate of decomposition of the methyl-substituted Criegee intermediate (relative to the dimethyl-substituted Criegee intermediate) is not as large as might be expected on density of states grounds alone because of the larger barrier to reaction for methyl-substituted Criegee intermediate, and therefore decreased tunneling in this system. Correspondingly, the decomposition of MVK-oxide is even slower than might be predicted solely based on the enhanced density of states because of the higher barrier (18.0 kcal mol^{-1}) in this case.

Canonical Rate Constants, k(T)

More important in atmospheric and combustion environments are thermal rate constants, k(T), since these quantities are particularly relevant when collisions with inert molecules scramble the population of individual energy states in reacting species. In these situations, a canonical rather than microcanonical description of the system is more appropriate. Microcanonical rate measurements, k(E), are, however, significant constraints on the determination of thermal rates, k(T). As we have noted above, k(E) measurements, and the associated RRKM calculations, provide stringent tests of the properties of the transition state, including the energetics, models for tunneling, and structures. They also test the adequacy of electronic structure methodology and anharmonic frequency analysis, as the vibrational frequencies and descriptions of low frequency internal rotors are important to an accurate calculation of the densities of states or sums of states in the reactants, products, and transition states. These same molecular quantities are also important in extending k(E) measurements to k(T) values. Having experimentally determined values of k(E) and a model for microcanonical unimolecular decay (RRKM theory) that is in quantitative agreement provides a confidence-building foundation for the determination of k(T).

The distribution of internal energies, *P(E,T)* (see equation 1) can be written within RRKM theory for a unimolecular reaction as,[45]

$$P(E,T)=\frac{1}{Q(T)}N(E)e^{-E/k_BT}, \tag{3}$$

where *Q(T)* is the canonical partition function. When inserted into equation (1) (and allowing for reactivity at energies below E_0, i.e., tunneling), we obtain for *k(T)* a proportionality to the Boltzmann weighted average of the microcanonical rates *k(E)* over a range of energies E,[83]

$$k(T)=\frac{1}{Q(T)}\int_0^\infty k(E)N(E)e^{-E/k_BT}dE \tag{4}$$

This expression, which in the limit of rapid internal energy transfer reduces to the transition state theory expression for the thermal rate constant, provides us with a conceptual means for judging the contributions of various energy ranges to the thermal rate. In the upper panel of Figure 6,[55] we show the calculated values of the k(E), N(E), and the Boltzmann factor for *syn*-CH_3CHOO – the terms comprising the integrand of equation 4 – evaluated at 300 K for the case in which rotations (J=0) are excluded from the RRKM calculations. The product of these three terms is shown in the lower panel at different temperatures, and represents the contributions, as a function of energy, of the microcanonical decay to the thermal rate.[55] Clearly, at temperatures of atmospheric importance, the thermal rate is dominated by decay pathways that occur significantly below the transition state energy of 5963 cm^{-1} (17.05 kcal mol^{-1}), highlighting the importance of quantum mechanical tunneling in these hydrogen-transfer mechanisms.

The importance of having measured k(E) values over a range of energies as a constraint on extrapolated k(T) rates is demonstrated in the case of *syn*-CH_3CHOO. We have noted previously that there is some scatter (~ 25-30%) in the experimentally determined k(E) values at energies near 4200 cm^{-1} that is not reproduced in the RRKM calculations although the RRKM calculations are in quantitative agreement with experimental measurements near the energy of the transition state. A simple adjustment to the Eckart potential used to model the tunneling is found to bring the RRKM calculations into better alignment with an average of the lower energy measurements.[55] For example, decreasing the imaginary frequency by 55 cm^{-1} and the barrier height by 20 cm^{-1} results in microcanonical rates near 4200 cm^{-1} that are 20% lower, while the calculated k(E) values near the transition state energy are affected only slightly (~2%).

From the perspective of thermal rates, these adjustments prove to be notable. The original set of Eckart parameters, when used to calculate the high-pressure k(T) at 298 K, resulted in a value of 166 s^{-1}.[46] The adjusted set of parameters results in a value of k(T) at 298 K of 122 s^{-1}.[55] Clearly, for this class of Criegee intermediates, documenting the microcanonical kinetic behavior in energy ranges where tunneling dominates the dynamics is critical to extracting reliable thermal kinetic parameters. Several other computational studies of the decay of *syn*-CH_3CHOO have been completed, with high-pressure values of k(T) at 298 K that range from 24.2 s^{-1} to 328 s^{-1}.[38, 66, 84] One comprehensive analysis estimates that k(T) at 298 K and 4 Torr is ≤ 250 s^{-1}.[18] Direct experimental measurement of the thermal unimolecular decay of stabilized *syn*-CH_3CHOO had been elusive until a very recent measurement of 182 ± 66 s^{-1} at 298 K.[85]

Equation (4) highlights the relationship between the k(T), k(E), and molecular properties of the reactant such as the density of states, N(E), and the canonical partition function Q(T). It is important to note that the averaging over energy and the density of states can lead to counter-intuitive trends in the thermal rates. For example, Figure 2 shows that for all energies, the dimethyl-substituted Criegee intermediate undergoes slower unimolecular decay than the methyl-substituted Criegee intermediate prepared with the same amount of internal energy. However, the calculated values of the appropriately averaged thermal rate constants, k(T), are actually *larger* for the dimethyl-substituted Criegee intermediate at temperatures important in the troposphere.[46] (The relevant values at 298 K for k(T) are 276 s^{-1} and 122 s^{-1} for dimethyl- and methyl-substituted Criegee intermediate, respectively, in the high-pressure limit.[55, 57]) As noted previously, equation (4) reduces to the transition state theory (TST) expression for the thermal rate constant in the limit of rapid intramolecular energy transfer. In the language of TST, this result arises because when thermalized the additional degrees of freedom present in the dimethyl-substituted species affect, roughly, the reactant and transition state partition functions to the same extent and it is only the lower barrier (~ 300 cm^{-1}; 0.9 kcal mol^{-1}) to reaction that drives the thermal rate higher for the dimethyl-substituted Criegee intermediate.[46] On the other hand, from RRKM theory, rates determined at single energies are sensitive to single values of the tunneling weighted sum-of-states in the transition state, $G^{\dagger}(E-E_0)$, and the density of states in the reactant, N(E) (see equation (2)). The differing sensitivity of the canonical and microcanonical rates on calculated properties highlights the value of considering the interplay between both types of experimental measurements and theoretical studies. The computed thermal unimolecular decay rate for $(CH_3)_2COO$ of 276 s^{-1} (298 K) has been further validated by experimental measurements yielding k(T) of 361 ± 49 s^{-1} (298 K)[86] and 305 ± 70 s^{-1} (293 K).[29]

The ethyl-substituted Criegee intermediate is found to have a thermal rate constant that is very close to that of the dimethyl-substituted molecule. For the ethyl-substituted Criegee intermediate, k(T=298 K) = 279 s^{-1}.[56] *Syn*-MVK-oxide has the lowest value for the microcanonical rate constant (see Figure 2), and the highest barrier to reaction. Based on the discussion above, we expect that the thermal rate constant will also be small. At 298 K, Barber, et al, find this value to be 33 s^{-1},[62] which is a Boltzmann weighted average value for the *syn-trans* (24 s^{-1}) and *syn-cis* (102 s^{-1}) conformers.[87] This result agrees well with a previous calculation, 50 s^{-1} at 298 K by Vereeckeen, *et al*.,[44] and is in qualitative agreement with the results of Kuwata et al., who find that the thermal rate for the *syn-trans*-conformer is 14.7 s^{-1}, while that of the *syn-cis*-conformer is 146 s^{-1}.[38] In all cases, the decay of *syn*-MVK-oxide at 298 K, and 1 atm pressure is within 1-10% of the high-pressure limit.[62]

Master equation modeling is also used to determine thermal rate constants over a range of pressure conditions. The inputs are molecular properties (vibrational frequencies, structures, energetic parameters) for the reactants, transition states, and products, as well as models for the collisions of reactive molecules with inert bath molecules (Lennard-Jones parameters and model parameters for collision-induced intramolecular energy transfer). For the methyl-substituted Criegee intermediate, solutions to the master equation show that the thermal rate constant at atmospheric pressure is within 0.5% of the high-pressure limit.[46] For the dimethyl-substituted Criegee intermediate, the deviation from the high-pressure limit is even smaller,[46] a result of the higher density of vibrational states, and thus more facile thermal energy exchange with the bath. With the exception of the unsubstituted CH_2OO,[66] Criegee intermediates appear to behave, kinetically, at or very near to the high-pressure limit under conditions appropriate to the troposphere. Even at 0.01 bar pressure, the thermal rate constant for unimolecular decay of the methyl-substituted Criegee intermediate is within 10% of the high-pressure limit.[46]

Master equation modeling has also proved to be a powerful tool in demonstrating the importance of tunneling in unimolecular decay in both chemically activated and thermalized Criegee intermediates. Drozd *et al.* carried out an extensive master equation study of the prompt and thermal unimolecular decay of the dimethyl substituted species, $(CH_3)_2COO$.[15] In this work, they examined first the collisional processes that control the stabilization of the nascent Criegee intermediates formed from decomposition of the primary ozonide (see Scheme 1). They found that tunneling plays a significant role in determining the yield of stabilized Criegee intermediates, counter-intuitively decreasing the yield by allowing lower energy chemically activated molecules to promptly decay prior to collisional relaxation. Drozd *et al.* also identified separable timescales for unimolecular decay of $(CH_3)_2COO$ to form OH radicals. Within 100 ns, prompt OH formation is complete, as is the formation of a population of collisionally thermalized Criegee intermediates. The decay of the latter occurs much slower, with a high-pressure, thermal rate constant of 276 s^{-1}. This difference in timescales provides an opportunity for important bimolecular reactions with the stabilized Criegee intermediates.

The high-pressure limit rate constants for the range of Criegee intermediates discussed in section II have been calculated over a range of temperatures to develop modified Arrhenius formulations. Figure 7 shows plots of the temperature dependence of the thermal rates constants of the four Criegee intermediates discussed here.[55-57, 62] Each of these plots exhibits substantial curvature, a testament to the importance of tunneling in the unimolecular decay of each molecule. This effect is further demonstrated by comparing the calculated thermal rate (298 K) from master equation studies in which tunneling is explicitly ignored. In this case, at high pressure, k(298 K) for *syn*-CH_3CHOO is found to be 1.4 s^{-1}, 2 orders of magnitude lower than the value (122 s^{-1}) determined when tunneling is incorporated.[55] For $(CH_3)_2COO$, the thermal rate k(298 K) drops to 8.6 s^{-1} if tunneling is neglected, which is ca. 30-times slower than the rate obtained with tunneling of 276 s^{-1}.[57]

IV. Alternative pathways for unimolecular decay of Criegee intermediates

1,4-hydrogen transfer is a mechanism for the unimolecular decomposition of Criegee intermediates that requires the presence of an alkyl substituent on the carbonyl carbon. All of the Criegee intermediates discussed in sections II and III meet this criterion. A second requirement is conformation: the $C=O^+-O^-$ group must be aligned towards one of the hydrogens of the alkyl group. This configuration defines the *syn*-conformer of these alkyl-substituted Criegee intermediates. In the *anti*-conformer, the $C=O^+-O^-$ group is aligned with the non-alkyl substituent on the carbonyl carbon.

Using these criteria, the unsubstituted Criegee intermediate, CH_2OO, is obviously not capable of 1,4 – hydrogen transfer. Similarly, the methyl- and ethyl-substituted Criegee intermediates have higher-energy *anti*-conformers, separated from the *syn*-conformer by a substantial activation barriers, ~ 35 kcal mol^{-1}.[38, 44] Figure 3 shows the structures of the *cis*- and *trans*-configurations of the *anti*-conformers of MVK-oxide. In these *anti*-conformer Criegee intermediates the alignment of the $C=O^{+}-O^{-}$ group is with the vinyl moiety; the sp^2 hybridization of the carbon atoms in this group make the barrier for transfer of a hydrogen atom prohibitively high.[44, 62] Finally, in Scheme 3, we show an additional four-carbon unsaturated Criegee intermediate produced in the ozonolysis of isoprene, methacrolein-oxide (MACR-oxide). Like MVK-oxide, MACR-oxide can adopt four conformations (see Figure 8),[88] but unlike MVK-oxide, none of the MACR-oxide conformers can undergo 1,4-hydrogen transfer.[89] In the remainder of this section, we review the alternative unimolecular reaction pathways predicted for these Criegee intermediates.

CH_2OO unimolecular dynamics

In the atmosphere, the unsubstituted Criegee intermediate CH_2OO is produced directly from the ozonolysis of ethene, and as one of the products in the ozonolysis of more complicated terminal alkenes (see, for example, Scheme 3, for the ozonolysis of isoprene). The decomposition of the primary ozonide formed from the reaction of ethene and ozone releases significant energy into products; one statistical model predicts an average nascent internal energy excitation in CH_2OO of 31 kcal mol^{-1}.[90] Quantum chemistry studies show that CH_2OO has two energetically accessible unimolecular decay paths: the ring-closing mechanism to form dioxirane depicted in Scheme 7 and bond fission to form HCO + OH.

Scheme 7: Unimolecular decay of CH_2OO proceeds via a high-energy ring closure to dioxirane.

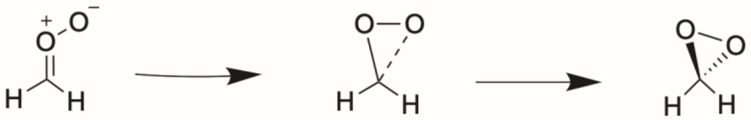

Bond fission, while exothermic by 7.4 kcal mol^{-1}, proceeds over a transition state that is calculated to exceed 31.5 kcal mol^{-1},[34, 66] and is likely feasible only for those Criegee intermediates with the highest levels of internal excitation. On the other hand, formation of dioxirane, which is exothermic by almost 24 kcal mol^{-1}, requires surmounting a transition state barrier of ca. 19 kcal mol^{-1}.[34, 66]

Under atmospheric conditions, unimolecular reaction of CH_2OO formed with significant internal excitation will compete with stabilization brought about by thermalizing collisions with inert gases such as N_2. The yield of stabilized CH_2OO from ethene ozonolysis has been examined theoretically and experimentally, as summarized recently.[90] The experimental values for the yield of stabilized CH_2OO range between 35 and 54%; the theoretical values arise from master-equation modeling based on differing levels of electronic structure calculations and range from 21 to 48%. It is difficult to draw definitive conclusions from the theoretical values in particular because of the varying methodologies represented. The lowest value, 21%, arises from a study by Olzmann, *et al.* that did not consider all of the reactive channels for chemically activated CH_2OO, and used transition state energies that were somewhat lower than more recent studies.[91] In contrast, Nguyen, *et al.* based their conclusion of a stabilized CH_2OO yield of 42% on a two-dimensional master-equation modeling study that explicitly considers the role of angular momentum in the reactivity of CH_2OO.[34] They suggest that angular momentum effects are responsible, at least in part, for the discrepancy with the results from the one-dimensional master-equation modeling study of Olzmann, *et al*.[91] Finally, Pfeifle, *et al*. combine ab initio direct dynamics trajectory calculations with one-dimensional master equation modeling on a new potential energy surface; the consensus yield of stabilized CH_2OO from this work is 48%.[90]

Reliable experimental measurements of the unimolecular decay of CH_2OO have proved to be difficult under thermal conditions because the decay is relatively slow and thus physical processes such as wall reactions and diffusion, and secondary chemical reaction may contribute to the experimental rates. Chhantyal-Pun *et al*. report an upper limit for the decay of CH_2OO at 293 K in 7-30 Torr of N_2 of 11.6 ± 8.0 s^{-1},[92] while Berndt *et al*. proposed an upper limit of 9.4 ± 1.7 s^{-1} at 293 K and 760 Torr.[93] In a more recent study, Berndt *et al*. refined their result to 0.19 ± 0.07 s^{-1} at 297 K and 1 bar pressure.[94] Stone *et al*., have most recently reported a unimolecular decay rate for CH_2OO at 298 K and 760 Torr of $1.1^{+1.5}_{-1.1} \times 10^{-3}$ s^{-1},[95] a value that is based on direct measurements of the unimolecular decay of CH_2OO at higher temperatures (and lower pressures) and extrapolated using master-equation modeling.

There have been few theoretical treatments of the thermal unimolecular decay of CH_2OO. A 2016 study by Long *et al.* found that the 298 K thermal decay to form dioxirane is 0.31 s^{-1} in the high-pressure limit,[66] comparing very favorably with the only other theoretical result, 0.3 s^{-1}.[91] Long *et al*. find, however, that under typical atmospheric conditions (298 K, 1 bar pressure), the thermal rate constant is significantly lower (*i.e*., far from the high-pressure limit), 0.072 s^{-1}.[66]

anti-CH_3CHOO dynamics

The unimolecular chemistry of *anti*-CH_3CHOO has been less documented, in general, than that of CH_2OO. There are no energy resolved measurements of the unimolecular decay of *anti*-CH_3CHOO, and thermal measurements of the unimolecular reactions of CH_3CHOO are assumed in most cases to measure the kinetics of a mixture of *syn*- and *anti*-conformers.[35] Kuwata, *et al*. have considered the unimolecular decay dynamics from a theoretical perspective, however.[38] In this work, master-equation modeling is used to derive thermal rate information. The exclusive reactive pathway for *anti*-CH_3CHOO is ring-closure to form a dioxirane structure shown in Scheme 8, with an activation barrier of 14.89 kcal mol^{-1} and a reaction exothermicity of 23.34 kcal mol^{-1}. *Anti*-conformers cannot isomerize to form *syn*-conformers. (The barrier to *anti*-*syn* isomerization is ~34.5 kcal mol^{-1}.[38]) Similarly, *anti*-CH_3CHOO has a high barrier (~30.1 kcal mol^{-1}) for a hydrogen-atom transfer reaction forming CH_3CO + OH radicals.[38] At 298 K, the high-pressure rate constant for the unimolecular decay of *anti*-CH_3CHOO is found to be 67.3 s^{-1}.[38] This rate is calculated to have a significant temperature dependence with the value dropping to 2.02 X 10^{-4} s^{-1} at 200 K. A second theoretical calculation by Long, *et al*. is largely in accord, providing a high-pressure thermal decay rate constant of 55.4 s^{-1} at 298 K.[66] (In this calculation, the dioxirane and CH_3CO + OH channel transition state energies are found to be 15.63 and 29.01 kcal mol^{-1}, respectively, in agreement with the results of Kuwata, *et al*.[38])

Scheme 8: Unimolecular decay of the less stable anti conformer of CH_3CHOO follows ring closure to dioxirane.

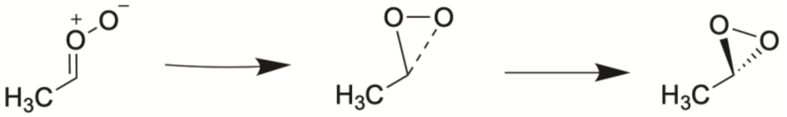

Long, *et al.*'s master-equation modeling shows that decay of *anti*-CH_3CHOO to the dioxirane form is in the high-pressure limit at temperatures of relevance to chemistry in the troposphere. For example, at 298 K, the thermal rate constant reaches half the high-pressure value at 0.199 bar. Vereecken *et al*., similarly report a high-pressure thermal (298 K) rate constant of 53 s^{-1} for the dioxirane forming reaction.[44]

anti-MVK-oxide dynamics

As noted previously, MVK-oxide exists in four conformations, two of which (*anti-cis* and *anti-trans*; see Figure 3) are not capable of participating in a 1,4 – hydrogen transfer reaction that will promptly yield OH radicals.[38, 62, 75] Just the same, these conformers have rich unimolecular chemistry. Kuwata *et al*. explored features of the potential energy surface, and found that, as in the case of CH_2OO and *anti*-CH_3CHOO, formation of dioxirane structures are possible, albeit with transition state energies that are 16.8 and 22.0 kcal mol^{-1} above the energy of the *anti-trans* and *anti-cis*-MVK-oxide conformers, respectively.[75] Uniquely, for the *anti-cis* conformer, is the possibility of an electrocyclic ring-closure reaction to form a 5-membered ring dioxole (*cyc*-$CH_2OOC(CH_3)CH$) shown in Scheme 9 with a relatively modest transition state energy of 11.0 kcal mol^{-1}.[75]

Scheme 9: Unimolecular decay of the anti-cis conformer of MVK-oxide follows a low energy ring closure pathway to dioxole.

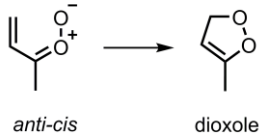

The reactions forming both of the cyclic products are substantially exothermic (>~ 20 kcal mol^{-1}). These results are largely consistent with higher level electronic structure calculations presented by Barber, *et al*., with a significant difference being that the barrier to the formation of dioxole is somewhat higher at 12.01 kcal mol^{-1}.[62] Kuwata, *et al*. describe master-equation studies that incorporate multiple reactive channels, leading to both dioxirane and dioxole structures, for the decomposition of *anti*-MVK-oxide. They find that dioxole is the favored product, consistent with its lower transition state barrier, and is predicted to have a larger yield than the dioxirane channel by an order of magnitude. However, there is not yet any direct experimental evidence of the dioxole product.

The infrared action spectroscopy study of Barber, *et al*. which determined k(E) for a vibrationally excited level in *syn-trans*-MVK-oxide also identified features in the infrared action spectrum that are ascribed to *anti*-MVK-oxide.[62] The observation of these features in the *action* spectrum means that excitation leads to the production of OH radicals following unimolecular reaction. Barber, *et al.* conclude that the most likely source of OH radicals is formation of dioxole following infrared excitation of *anti*-MVK-oxide. (The photon energy used, ~5900 cm^{-1} (16.9 kcal mol^{-1}), far exceeds the ~ 8 kcal mol^{-1} barrier to *cis-trans* isomerization, so that conformation label is not needed). Infrared excited *anti*-MVK-oxide will have sufficient energy to rearrange to dioxole, which is formed with more than 25 kcal mol^{-1} of internal energy. This is adequate internal excitation for a multi-step process involving a ring-opening, a hydrogen-transfer, tautomerization, and release of OH products; alternatively, it is possible that OH is formed via a UV-assisted photodissociation pathway.[62] Barber, *et al*. calculate the thermal rate at 298 K for the first step in the process – the unimolecular decay of *anti-cis*-MVK-oxide to dioxole – to be a relatively fast 2140 s^{-1},[62] as a result of the low barrier to the reaction. This result is a Boltzmann average of the *anti-trans*-MVK-oxide to dioxole thermal rate (2.1×10^3 s^{-1}) and the *anti-cis*-MVK-oxide to dioxole rate (3.3×10^3 s^{-1}).[87]

Vereecken, *et al*. reports thermal rate constants for both the dioxirane and dioxole reaction channels from *anti*-MVK-oxide.[44] At 298 K, these authors find that the formation of dioxole from *anti*-MVK-oxide proceeds with a high-pressure rate constant of 7.7×10^3 s^{-1}, substantially higher than that found by Barber, *et al*. In contrast, formation of dioxirane is much slower at 298 K, with k(T) values of 4.0×10^{-3} s^{-1} for the *syn* conformers, and 1.6 s^{-1} for the *anti*-conformers.

Methacrolein-oxide dynamics

Scheme 3 outlines the reaction sequence in which MACR-oxide emerges as one of the Criegee intermediates formed in the ozonolysis of isoprene.[72, 74] Like MVK-oxide, this Criegee intermediate exists as four conformers: *syn*- and *anti*-, which differ in the rotation about the C = O bond, and *cis*- and *trans*-, which differ in rotation about the C – C bond adjacent to the carbonyl group.[88, 89] These four conformers have ground state energies that lie within 3.2 kcal mol^{-1} of one another, with the *anti-trans* the most stable and the *anti-cis* the least stable.[88] (See Figure 8.)

Unlike MVK-oxide, however, none of the conformers are capable of forming 1,4 – hydrogen transfer transition states, since these molecules lack alkyl groups α to the carbonyl carbon. The unimolecular dynamics of MACR-oxide are thought to be dominated, therefore, by the formation of dioxirane structures, or in the case of the *syn-cis*-conformer, ring closure to form a dioxole molecule. The transition state energies to form dioxirane compounds are calculated to range from 13.9 to 25.3 kcal mol^{-1}, while the energy required to reach the dioxole transition state is relatively small, 11.9 kcal mol^{-1}.[89] The unimolecular chemistry of the MACR-oxide conformer (*syn-cis*) is predicted to follow the dioxole channel and should be quite similar to that of the *anti*-conformers of MVK-oxide.

Vereecken, *et al.* report a calculated high-pressure limit thermal rate constant for the cyclization reaction of *syn-cis*-MACR-oxide to dioxole at 298 K.[44] The result is 2.5×10^3 s^{-1}, the same order of magnitude predicted for MVK-oxide. The formation of the dioxirane is significantly slower, consistent with the higher barriers to reaction, and is conformer dependent. In these cases, k(T = 298 K) is 0.35 s^{-1} for the *syn*-conformers, and 10 s^{-1} for the *anti*-conformers. Kuwata, *et al.*, carried out master-equation modeling on a chemically activated distribution of MACR-oxide Criegee intermediates that obtain their internal energy distribution from the dissociation of the isoprene primary ozonide.[89] In this simulation, at 298 K and 1 atm of N_2 as buffer gas, the dominant products were the dioxirane molecules, likely favored because they are the only accessible pathway for the lowest energy *anti-trans*-conformer. (As in MVK-oxide, the *syn-anti* isomerization barrier in MACR-oxide is quite high, $>\sim$ 20 kcal mol^{-1}.) Formation of the dioxole species was found to be a significant secondary product.

Additional unimolecular pathways

As Criegee intermediate substituents become more complex, additional unimolecular pathways are predicted to become available, although these are significantly less well characterized. Vereecken *et al*. theoretically examined the extensive unimolecular chemistry possible for Criegee intermediates and concluded that a few chemical reaction classes are most relevant.[44] Moreover, they find that for a given structure and conformer, a single reaction pathway is generally dominant. Specifically, the dominant unimolecular pathways include 1,4 hydrogen migration to vinyl hydroperoxide and OH products, 1,3 ring closure to dioxirane, and 1,5 ring closure to dioxole channels, as discussed previously in this review. In addition, they predict a substantial increase the rate of 1,4 H-migration for γ-unsaturated Criegee intermediates due to allyl resonance stabilization of both the transition state and the conjugated vinyl hydroperoxide product. They also predict very low transition state barriers and exceedingly rapid unimolecular decay rates for β-unsaturated Criegee intermediates that can undergo allyl-1,6-H migration to a conjugated vinyl hydroperoxide product. This is attributed to stabilization effects of the conjugated π-system and alleviated ring strain in the transition state that enables rapid H-atom migration over a large distance. In both cases, the hydroperoxide product will predominantly dissociate to OH radicals. For Criegee intermediates with hetero-substituted functionality, such as a C=O group arising from ozonolysis of endocyclic alkenes (e.g. cyclic monoterpenes), additional very rapid ring closure reactions are possible. Long *et al*. recently predicted a very fast unimolecular decay pathway for 5 and 6 carbon Criegee intermediates containing an aldehyde (CH=O) group, which involves ring closure to form bicyclic structures.[96] This is analogous to the formation of secondary ozonides (SOZ) in bimolecular reactions of Criegee intermediates with molecules containing a carbonyl (C=O) group, but may be possible for other functionalities as well. Vereecken and Francisco have suggested that at least 6 connecting carbon atoms between the oxide and carbonyl moieties will be required for efficient internal SOZ formation.[97]

V. Atmospheric significance of thermal rates of decay of Criegee intermediates

Criegee intermediates play an important role in the overall oxidation chemistry in the troposphere. The unimolecular decomposition of the Criegee intermediates discussed in the preceding sections has significance as a non-photolytic source of OH radicals.[5-10] The ultimate fate of the Criegee intermediates also depends on the competition between unimolecular decay and bimolecular reaction with other species in the atmosphere. Thus the thermal rate of unimolecular decay serves to modulate the bimolecular chemistry.

The substituents and conformational form of the Criegee intermediates are observed to play an important role in determining the bimolecular chemistry of Criegee intermediates, and thus the competition with thermal rates of unimolecular decay. For example, in *syn*-CH_3CHOO, for which the 1,4-hydrogen transfer leads to the production of OH with a thermal rate (298 K) that is on the order of 100 s^{-1},[9] the bimolecular reaction with water is quite slow. Experimental measurements are only able to place an upper limit on the bimolecular rate constant, either $<4 \times 10^{-15}$ cm^3 s^{-1} or 2×10^{-16} cm^3 s^{-1}.[18, 98] Theoretical estimates range from 2.1×10^{-18} to 1.2×10^{-20} cm^3 s^{-1}.[26, 66, 99-101] Long *et al.*, using a theoretical estimate for both the unimolecular decay of *syn*-CH_3CHOO, and an average partial pressure of water vapor at the Earth's surface, deduced an atmospheric lifetime due to unimolecular decay of 4.5 milliseconds, while the lifetime due to bimolecular reaction with water is 19 seconds.[66] Under atmospheric conditions, water dimers exist in non-negligible concentrations, and are found to have significantly higher reactivity with *syn*-CH_3CHOO. For example, the bimolecular rate constant in calculated to be 2.56 X 10^{-14} cm^3 s^{-1},[26] several orders of magnitude larger than the rate constant with water monomer. However, since the concentration of the dimer remains 5-7 orders of magnitude smaller than the monomer, the lifetime associated with *syn*-CH_3CHOO due to the bimolecular reaction with the dimer is of the order of 10 seconds at low altitudes.[66]

In contrast, *anti*-CH_3CHOO has a more modest rate of thermal unimolecular decay, and a much faster bimolecular reaction with both water monomer and dimer. The consensus bimolecular experimental rate constants with water monomer are between 1 X 10^{-14} and 2.5 X 10^{-14} cm^3 s^{-1},[18, 98, 102, 103] with theoretical values that range between 1.7 X 10^{-13} and 6.7 X 10^{-16} cm^3 s^{-1}.[26, 66, 99, 100] The increase in the reactivity of the *anti*-conformer is ascribed primarily to electronic effects associated with increased stabilization of the Criegee-water monomer complex transition state. As before, Long *et al*., determined effective atmospheric lifetimes for *anti*-CH_3CHOO under tropospheric conditions; the unimolecular decay lifetime is found to be 49 milliseconds, while the lifetime due to the bimolecular reaction with water monomer is 0.56 milliseconds.[66] The faster experimentally determined rate constants for the reaction with water suggest an even shorter lifetime (~0.1 – 0.2 milliseconds) for *anti*-CH_3CHOO. The bimolecular rate constant with water dimer is calculated to be 1.60 X 10^{-11} cm^3 s^{-1}, significantly larger than that for the water monomer.[26]

The structural sensitivity exhibited in the unimolecular and bimolecular reactions of CH_3CHOO is not confined to this Criegee intermediate,[26, 66, 99-101] or to the reaction with water.[35] Similar results are found in the reactions with water dimer[101] and alcohols,[30], and for Criegee intermediates as large as MVK-oxide and MACR-oxide.[38, 44, 62, 75, 87, 89, 100, 101, 104]

Recently, the question has been raised as to whether unimolecular decay,[44] along with reaction with relatively abundant water vapor, will limit the atmospheric concentration of stabilized Criegee intermediates (estimated at 10^4/cm^3)[44, 105] and therefore their global impact in secondary bimolecular chemistry. This issue will not be fully resolved until we obtain a more complete understanding of the interplay of the unimolecular and bimolecular chemistry of the full range of Criegee intermediates of atmospheric relevance (including those derived from biogenic alkenes, e.g. isoprene, α-pinene and β-pinene). In the atmosphere, it is likely that only water, SO_2, and NO_x are of sufficient concentration to act as significant sinks for Criegee intermediates.[10] However, Criegee intermediates can still be substantial contributors to formation or loss of other atmospheric species. For example, recent global atmospheric models show that oxidation of SO_2 by Criegee intermediates in heavily forested regions may be an important source of SO_3, H_2SO_4, and ultimately secondary organic aerosols.[31-33] It is important to note that *syn*-methyl vinyl ketone oxide (*syn*-MVK-oxide), derived from ozonolysis of abundant isoprene, has a relatively slow unimolecular rate constant,[62, 87] and negligible bimolecular rate constants with water monomers and dimers ($< 2 \text{ X } 10^{-17}$ cm^3 s^{-1} with water monomers; $< 5 \text{ X } 10^{-14}$ cm^3 s^{-1} with water dimers[101]) allowing it to survive in high humidity environments. As a result, this Criegee intermediate is expected to be important in bimolecular chemistry with other, less abundant atmospheric species including SO_2 and carboxylic acids.[87]

Many of the studies described here and those carried out by other investigators to date have only scratched the surface in terms of atmospherically important Criegee intermediates. The focus of the overwhelming majority of this work has been on Criegee intermediates containing one to four carbon atoms, i.e., those intermediates that arise from alkenes as simple as ethene or as complex as isoprene. The latter in particular are likely to be a continuing focus of research given the abundance of isoprene in the environment, and the significance of understanding the ozonolysis mechanism and products (see Scheme 3). Isoprene is the most abundant volatile organic compound in the atmosphere (aside from methane) with biogenic and anthropogenic emissions of ~ 600 Tg per year.[1, 2] While only about 10% of all isoprene in the atmosphere undergoes ozonolysis,[72] the sheer magnitude of the emissions will likely make the resulting Criegee intermediates (CH_2OO, methyl vinyl ketone-oxide, methacrolein-oxide) significant players in subsequent atmospheric chemistry.

There are, however, many abundant naturally occurring alkenes, and only a few studies have considered the reactivity of the Criegee intermediates that result from the ozonolysis of α- and β-pinene,[106-108] and limonene,[109] and, on a theoretical basis, intermediates possessing bifunctional character.[14, 96, 110] These investigations highlight the general principle that there is an abundance of naturally occurring alkenes exhibiting significant structural diversity – ranging from simple straight-chain hydrocarbons (1- and 2-butene, 1- and 2-hexene) to the terpenoids.[3] The possibilities for the further experimental and theoretical study of the unimolecular decay of Criegee intermediates, at the microcanonical and thermal rate level, appears nearly unlimited.

Acknowledgements

The original research was primarily supported by National Science Foundation Grants CHE-1362835 and CHE-1664572 (to M.I.L.). This review is an overview of the outstanding research conducted by many talented graduate students and postdoctoral scholars on Criegee intermediates including Victoria P. Barber, Trisha K. Bhagde, Joseph M. Beames, Greg T. Drozd, Vincent J. Esposito, Yi Fang, Amy M. Green, Nathan M. Kidwell, Julia H. Lehman, Hongwei Li, Fang Liu, Barbara Marchetti, Shubhrangshu Pandit, Anne Schou Reinholdt, Michael F. Vansco, and Guanghan Wang. M.I.L. also thanks senior collaborators Anne B. McCoy (University of Washington), Stephen J. Klippenstein (Argonne National Laboratory), and Patrick Walsh (University of Pennsylvania). T.A.S. is grateful to Swarthmore College for generous sabbatical leave support.

References

1. K. Sindelarova, C. Granier, I. Bouarar, A. Guenther, S. Tilmes, T. Stavrakou, J. F. Müller, U. Kuhn, P. Stefani and W. Knorr, Atmos. Chem. Phys. **14**, 9317 (2014).
2. M. A. H. Khan, B.-L. Schlich, M. E. Jenkin, B. M. A. Shallcross, K. Moseley, C. Walker, W. C. Morris, R. G. Derwent, C. J. Percival and D. E. Shallcross, Atmos **9**, 387 (2018).
3. B. J. Finlayson-Pitts and J. N. Pitts, *Chemistry of the Upper and Lower Atmosphere*. (Academic Press, San Diego, 2000).
4. J. G. Calvert, R. Atkinson, J. A. Kerr, S. Madronich, G. K. Moortgat, T. J. Wallington and G. Yarwood, *The Mechanisms of Atmospheric Oxidation of the Alkenes*. (Oxford University Press, Oxford, 2000).
5. R. M. Harrison, J. Yin, R. M. Tilling, X. Cai, P. W. Seakins, J. R. Hopkins, D. L. Lansley, A. C. Lewis, M. C. Hunter, D. E. Heard, L. J. Carpenter, D. J. Creasey, J. D. Lee, M. J. Pilling, N. Carslaw, K. M. Emmerson, A. Redington, R. G. Derwent, D. Ryall, G. Mills and S. A. Penkett, Sci. Total Environ. **360**, 5 (2006).
6. K. M. Emmerson, N. Carslaw, D. C. Carslaw, J. D. Lee, G. McFiggans, W. J. Bloss, T. Gravestock, D. E. Heard, J. Hopkins, T. Ingham, M. J. Pilling, S. C. Smith, M. Jacob and P. S. Monks, Atmos. Chem. Phys. **7**, 167 (2007).
7. K. M. Emmerson and N. Carslaw, Atmos. Environ. **43**, 3220 (2009).
8. Y. F. Elshorbany, R. Kurtenbach, P. Wiesen, E. Lissi, M. Rubio, G. Villena, E. Gramsch, A. R. Rickard, M. J. Pilling and J. Kleffmann, Atmos. Chem. Phys. **9**, 2257 (2009).
9. C. A. Taatjes, D. E. Shallcross and C. J. Percival, Phys. Chem. Chem. Phys. **16**, 1704 (2014).
10. M. A. H. Khan, C. J. Percival, R. L. Caravan, C. A. Taatjes and D. E. Shallcross, Environmental Science: Processes & Impacts **20**, 437 (2018).
11. D. Johnson and G. Marston, Chem. Soc. Rev. **37**, 699 (2008).
12. J. H. Kroll, J. S. Clarke, N. M. Donahue, J. G. Anderson and K. L. Demerjian, J. Phys. Chem. A **105**, 1554 (2001).
13. J. H. Kroll, T. F. Hanisco, N. M. Donahue, K. L. Demerjian and J. G. Anderson, Geophys. Res. Lett. **28**, 3863 (2001).
14. N. M. Donahue, G. T. Drozd, S. A. Epstein, A. A. Presto and J. H. Kroll, Phys. Chem. Chem. Phys. **13**, 10848 (2011).
15. G. T. Drozd, T. Kurtén, N. M. Donahue and M. I. Lester, J. Phys. Chem. A **121**, 6036 (2017).
16. R. L. Mauldin III, T. Berndt, M. Sipilä, P. Paasonen, T. Petäjä, S. Kim, T. Kurtén, F. Stratmann, V. M. Kerminen and M. Kulmala, Nature **488**, 193 (2012).
17. O. Welz, J. D. Savee, D. L. Osborn, S. S. Vasu, C. J. Percival, D. E. Shallcross and C. A. Taatjes, Science **335**, 204 (2012).
18. C. A. Taatjes, O. Welz, A. J. Eskola, J. D. Savee, A. M. Scheer, D. E. Shallcross, B. Rotavera, E. P. F. Lee, J. M. Dyke, D. K. W. Mok, D. L. Osborn and C. J. Percival, Science **340**, 177 (2013).
19. B. Ouyang, M. W. McLeod, R. L. Jones and W. J. Bloss, Phys. Chem. Chem. Phys. **15**, 17070 (2013).
20. L. Sheps, J. Phys. Chem. Lett. **4**, 4201 (2013).
21. Y. Liu, K. D. Bayes and S. P. Sander, J. Phys. Chem. A **118**, 741 (2014).
22. W. Chao, J.-T. Hsieh, C.-H. Chang and J. J.-M. Lin, Science **347**, 751 (2015).

23. T. R. Lewis, M. A. Blitz, D. E. Heard and P. W. Seakins, Phys. Chem. Chem. Phys. **17**, 4859 (2015).
24. H.-L. Huang, W. Chao and J. J.-M. Lin, Proc. Natl. Acad. Sci. **112**, 10857 (2015).
25. J. P. Hakala and N. M. Donahue, J. Phys. Chem. A **120**, 2173 (2016).
26. L.-C. Lin, H.-T. Chang, C.-H. Chang, W. Chao, M. C. Smith, C.-H. Chang, J. Jr-Min Lin and K. Takahashi, Phys. Chem. Chem. Phys. **18**, 4557 (2016).
27. L. Vereecken and H. M. T. Nguyen, Int. J. Chem. Kinet. **49**, 752 (2017).
28. R. L. Caravan, M. A. H. Khan, B. Rotavera, E. Papajak, I. O. Antonov, M.-W. Chen, K. Au, W. Chao, D. L. Osborn, J. J.-M. Lin, C. J. Percival, D. E. Shallcross and C. A. Taatjes, Faraday Discuss. **200**, 313 (2017).
29. R. Chhantyal-Pun, O. Welz, J. D. Savee, A. J. Eskola, E. P. F. Lee, L. Blacker, H. R. Hill, M. Ashcroft, M. A. H. Khan, G. C. Lloyd-Jones, L. Evans, B. Rotavera, H. Huang, D. L. Osborn, D. K. W. Mok, J. M. Dyke, D. E. Shallcross, C. J. Percival, A. J. Orr-Ewing and C. A. Taatjes, J. Phys. Chem. A **121**, 4 (2017).
30. N. A. I. Watson, J. A. Black, T. M. Stonelake, P. J. Knowles and J. M. Beames, J. Phys. Chem. A **123**, 218 (2019).
31. C. J. Percival, O. Welz, A. J. Eskola, J. D. Savee, D. L. Osborn, D. O. Topping, D. Lowe, S. R. Utembe, A. Bacak, G. M c Figgans, M. C. Cooke, P. Xiao, A. T. Archibald †, M. E. Jenkin, R. G. Derwent, I. Riipinen, D. W. K. Mok, E. P. F. Lee, J. M. Dyke, C. A. Taatjes and D. E. Shallcross, Faraday Discuss. **165**, 45 (2013).
32. T. F. Mentel, M. Springer, M. Ehn, E. Kleist, I. Pullinen, T. Kurtén, M. Rissanen, A. Wahner and J. Wildt, Atmos. Chem. Phys. **15**, 6745 (2015).
33. R. Chhantyal-Pun, B. Rotavera, M. R. McGillen, M. A. H. Khan, A. J. Eskola, R. L. Caravan, L. Blacker, D. P. Tew, D. L. Osborn, C. J. Percival, C. A. Taatjes, D. E. Shallcross and A. J. Orr-Ewing, ACS Earth and Space Chemistry **2**, 833 (2018).
34. T. L. Nguyen, H. Lee, D. A. Matthews, M. C. McCarthy and J. F. Stanton, J. Phys. Chem. A **119**, 5524 (2015).
35. D. E. Shallcross, M. A. H. Khan, C. A. Taatjes and C. J. Percival, in *Advances in Atmospheric Chemistry* (2019), pp. 319.
36. L. Sheps, B. Rotavera, A. J. Eskola, D. L. Osborn, C. A. Taatjes, K. Au, D. E. Shallcross, M. A. H. Khan and C. J. Percival, Phys. Chem. Chem. Phys. **19**, 21970 (2017).
37. M. S. Alam, M. Camredon, A. R. Rickard, T. Carr, K. P. Wyche, K. E. Hornsby, P. S. Monks and W. J. Bloss, Phys. Chem. Chem. Phys. **13**, 11002 (2011).
38. K. T. Kuwata, M. R. Hermes, M. J. Carlson and C. K. Zogg, J. Phys. Chem. A **114**, 9192 (2010).
39. D. L. Osborn and C. A. Taatjes, Int. Rev. Phys. Chem. **34**, 309 (2015).
40. Y.-P. Lee, J. Chem. Phys. **143**, 020901 (2015).
41. C. A. Taatjes, Annu. Rev. Phys. Chem. **68**, 183 (2017).
42. J. Jr-Min Lin and W. Chao, Chem. Soc. Rev. **46**, 7483 (2017).
43. M. I. Lester and S. J. Klippenstein, Acc. Chem. Res. **51**, 978 (2018).
44. L. Vereecken, A. Novelli and D. Taraborrelli, Phys. Chem. Chem. Phys. **19**, 31599 (2017).
45. T. Baer and W. L. Hase, *Unimolecular Reaction Dynamics Theory and Experiments*. (Oxford University Press, New York, 1996).
46. Y. Fang, F. Liu, V. P. Barber, S. J. Klippenstein, A. B. McCoy and M. I. Lester, J. Chem. Phys. **144**, 061102 (2016).

47. J. M. Beames, F. Liu, L. Lu and M. I. Lester, J. Am. Chem. Soc. **134**, 20045 (2012).
48. J. H. Lehman, H. Li, J. M. Beames and M. I. Lester, J. Chem. Phys. **139**, 141103 (2013).
49. F. Liu, J. M. Beames, A. S. Petit, A. B. McCoy and M. I. Lester, Science **345**, 1596 (2014).
50. F. Liu, J. M. Beames and M. I. Lester, J. Chem. Phys. **141**, 234312 (2014).
51. F. Liu, J. M. Beames, A. M. Green and M. I. Lester, J. Phys. Chem. A **118**, 2298 (2014).
52. H. Li, Y. Fang, N. M. Kidwell, J. M. Beames and M. I. Lester, J. Phys. Chem. A **119**, 8328 (2015).
53. H. Li, Y. Fang, J. M. Beames and M. I. Lester, J. Chem. Phys. **142**, 214312 (2015).
54. E. P. F. Lee, D. K. W. Mok, D. E. Shallcross, C. J. Percival, D. L. Osborn, C. A. Taatjes and J. M. Dyke, Chem. Eur. J. **18**, 12411 (2012).
55. Y. Fang, F. Liu, V. P. Barber, S. J. Klippenstein, A. B. McCoy and M. I. Lester, J. Chem. Phys. **145**, 234308 (2016).
56. Y. Fang, F. Liu, S. J. Klippenstein and M. I. Lester, J. Chem. Phys. **145**, 044312 (2016).
57. Y. Fang, V. P. Barber, S. J. Klippenstein, A. B. McCoy and M. I. Lester, J. Chem. Phys. **146**, 134307 (2017).
58. A. M. Green, V. P. Barber, Y. Fang, S. J. Klippenstein and M. I. Lester, Proc. Natl. Acad. Sci. **114**, 12372 (2017).
59. V. P. Barber, S. Pandit, V. J. Esposito, A. B. McCoy and M. I. Lester, J. Phys. Chem. A **123**, 2559 (2019).
60. N. M. Kidwell, H. Li, X. Wang, J. M. Bowman and M. I. Lester, Nat. Chem. **8**, 509 (2016).
61. H. Li, N. M. Kidwell, X. Wang, J. M. Bowman and M. I. Lester, J. Chem. Phys. **145**, 104307 (2016).
62. V. P. Barber, S. Pandit, A. M. Green, N. Trongsiriwat, P. J. Walsh, S. J. Klippenstein and M. I. Lester, J. Am. Chem. Soc. **140**, 10866 (2018).
63. V. P. Barber, A. S. Hansen, S. J. Klippenstein and M. I. Lester, to be submitted (2019).
64. M. Nakajima and Y. Endo, J. Chem. Phys. **140**, 011101 (2014).
65. M. Nakajima, Q. Yue and Y. Endo, J. Mol. Spectrosc. **310**, 109 (2015).
66. B. Long, J. L. Bao and D. G. Truhlar, J. Am. Chem. Soc. **138**, 14409 (2016).
67. K. K. Lehmann, G. Scoles and B. H. Pate, Annu. Rev. Phys. Chem. **45**, 241 (1994).
68. H. S. Yoo, M. J. DeWitt and B. H. Pate, J. Phys. Chem. A **108**, 1348 (2004).
69. K. T. Kuwata, L. Luu, A. B. Weberg, K. Huang, A. J. Parsons, L. A. Peebles, N. B. Rackstraw and M. J. Kim, J. Phys. Chem. A **122**, 2485 (2018).
70. C. A. Taatjes, F. Liu, B. Rotavera, M. Kumar, R. Caravan, D. L. Osborn, W. H. Thompson and M. I. Lester, J. Phys. Chem. A **121**, 16 (2017).
71. C. Cabezas, J.-C. Guillemin and Y. Endo, J. Chem. Phys. **145**, 224314 (2016).
72. T. B. Nguyen, G. S. Tyndall, J. D. Crounse, A. P. Teng, K. H. Bates, R. H. Schwantes, M. M. Coggon, L. Zhang, P. Feiner, D. O. Milller, K. M. Skog, J. C. Rivera-Rios, M. Dorris, K. F. Olson, A. Koss, R. J. Wild, S. S. Brown, A. H. Goldstein, J. A. de Gouw, W. H. Brune, F. N. Keutsch, J. H. Seinfeld and P. O. Wennberg, Phys. Chem. Chem. Phys. **18**, 10241 (2016).
73. D. Zhang, W. Lei and R. Zhang, Chem. Phys. Lett. **358**, 171 (2002).
74. P. O. Wennberg, K. H. Bates, J. D. Crounse, L. G. Dodson, R. C. McVay, L. A. Mertens, T. B. Nguyen, E. Praske, R. H. Schwantes, M. D. Smarte, J. M. St Clair, A. P. Teng, X. Zhang and J. H. Seinfeld, Chem. Rev. **118**, 3337 (2018).

75. K. T. Kuwata, L. C. Valin and A. D. Converse, J. Phys. Chem. A **109**, 10725 (2005).
76. H. S. Johnston and J. Heicklen, J. Phys. Chem. **66**, 532 (1962).
77. W. H. Miller, R. Hernandez, C. B. Moore and W. F. Polik, J. Chem. Phys. **93**, 5657 (1990).
78. multiwell, J. R. Barker, T. L. Nguyen, J. F. Stanton, C. Aieta, M. Ceotto, F. Gabas, T. J. D. Kumar, C. G. L. Li, L. L. Lohr, A. Maranzana, N. F. Ortiz, J. M. Preses, J. M. Simmie, J. A. Sonk, and P. J. Stimac; MultiWell-2019 Software Suite; J. R. Barker, University of Michigan, Ann Arbor, Michigan, USA, (2019); http://clasp-research.engin.umich.edu/multiwell/.
79. T. L. Nguyen, J. F. Stanton and J. R. Barker, Chem. Phys. Lett. **499**, 9 (2010).
80. T. L. Nguyen, J. F. Stanton and J. R. Barker, J. Phys. Chem. A **115**, 5118 (2011).
81. B. Long, J. L. Bao and D. G. Truhlar, Proc. Natl. Acad. Sci. **115**, 6135 (2018).
82. A. F. Wagner, J. Phys. Chem. A **117**, 13089 (2013).
83. R. D. Levine, *Molecular reaction dynamics*. (Cambridge University Press, New York, 2009).
84. T. L. Nguyen, L. McCaslin, M. C. McCarthy and J. F. Stanton, J. Chem. Phys. **145**, 131102 (2016).
85. X. Zhou, Y. Liu, W. Dong and X. Yang, J. Phys. Chem. Lett. **10**, 4817 (2019).
86. M. C. Smith, W. Chao, K. Takahashi, K. A. Boering and J. J.-M. Lin, J. Phys. Chem. A **120**, 4789 (2016).
87. R. L. Caravan, M. F. Vansco, K. Au, M. A. H. Khan, Y.-L. Li, F. A. F. Winiberg, K. Zuraski, Y.-H. Lin, W. Chao, N. Trongsiriwat, P. J. Walsh, D. L. Osborn, C. J. Percival, J. J.-M. Lin, D. E. Shallcross, L. Sheps, S. J. Klippenstein, C. A. Taatjes and M. I. Lester, Proc. Natl. Acad. Sci., submitted (2019).
88. M. F. Vansco, B. Marchetti, N. Trongsiriwat, G. Wang, T. Bhagde, P. J. Walsh, S. J. Klippenstein and M. I. Lester, J. Am. Chem. Soc. **141**, 15058 (2019).
89. K. T. Kuwata and L. C. Valin, Chem. Phys. Lett. **451**, 186 (2008).
90. M. Pfeifle, Y.-T. Ma, A. W. Jasper, L. B. Harding, W. L. Hase and S. J. Klippenstein, J. Chem. Phys. **148**, 174306 (2018).
91. M. Olzmann, E. Kraka, D. Cremer, R. Gutbrod and S. Andersson, J. Phys. Chem. A **101**, 9421 (1997).
92. R. Chhantyal-Pun, A. Davey, D. E. Shallcross, C. J. Percival and A. J. Orr-Ewing, Phys. Chem. Chem. Phys. **17**, 3617 (2015).
93. T. Berndt, J. Voigtlander, F. Stratmann, H. Junninen, R. L. Mauldin Iii, M. Sipila, M. Kulmala and H. Herrmann, Phys. Chem. Chem. Phys. **16**, 19130 (2014).
94. T. Berndt, R. Kaethner, J. Voigtlander, F. Stratmann, M. Pfeifle, P. Reichle, M. Sipila, M. Kulmala and M. Olzmann, Phys. Chem. Chem. Phys. **17**, 19862 (2015).
95. D. Stone, K. Au, S. Sime, D. J. Medeiros, M. Blitz, P. W. Seakins, Z. Decker and L. Sheps, Phys. Chem. Chem. Phys. **20**, 24940 (2018).
96. B. Long, J. L. Bao and D. G. Truhlar, Nat. Comm. **10**, 2003 (2019).
97. L. Vereecken and J. S. Francisco, Chem. Soc. Rev. **41**, 6259 (2012).
98. L. Sheps, A. M. Scully and K. Au, Phys. Chem. Chem. Phys. **16**, 26701 (2014).
99. A. B. Ryzhkov and P. A. Ariya, Phys. Chem. Chem. Phys. **6**, 5042 (2004).
100. J. M. Anglada, J. Gonzalez and M. Torrent-Sucarrat, Phys. Chem. Chem. Phys. **13**, 13034 (2011).
101. J. M. Anglada and A. Solé, Phys. Chem. Chem. Phys. **18**, 17698 (2016).

102. M. J. Newland, A. R. Rickard, M. S. Alam, L. Vereecken, A. Munoz, M. Rodenas and W. J. Bloss, Phys. Chem. Chem. Phys. **17**, 4076 (2015).
103. L.-C. Lin, W. Chao, C.-H. Chang, K. Takahashi and J. J.-M. Lin, Phys. Chem. Chem. Phys. **18**, 28189 (2016).
104. M. F. Vansco, B. Marchetti and M. I. Lester, J. Chem. Phys. **149**, 244309 (2018).
105. R. Chhantyal-Pun, M. A. H. Khan, R. Martin, N. Zachhuber, Z. J. Buras, C. J. Percival, D. E. Shallcross and A. J. Orr-Ewing, ACS Earth and Space Chemistry (2019).
106. J. Ahrens, P. T. M. Carlsson, N. Hertl, M. Olzmann, M. Pfeifle, J. L. Wolf and T. Zeuch, Angew. Chem. Int. Ed. **53**, 715 (2014).
107. X.-X. Lin, Y.-R. Liu, T. Huang, K.-M. Xu, Y. Zhang, S. Jiang, Y.-B. Gai, W.-J. Zhang and W. Huang, RSC Advances **4**, 28490 (2014).
108. C. Giorio, S. J. Campbell, M. Bruschi, F. Tampieri, A. Barbon, A. Toffoletti, A. Tapparo, C. Paijens, A. J. Wedlake, P. Grice, D. J. Howe and M. Kalberer, J. Am. Chem. Soc. **139**, 3999 (2017).
109. M. J. Newland, A. R. Rickard, T. Sherwen, M. J. Evans, L. Vereecken, A. Muñoz, M. Ródenas and W. J. Bloss, Atmos. Chem. Phys. **18**, 6095 (2018).
110. K. T. Kuwata, B. J. Kujala, Z. W. Morrow and E. Tonc, Comput. Theor. Chem. **965**, 305 (2011).

Table 1: 1,4 – Hydrogen shift pathways: unimolecular decay stationary points

Energies relative to the Criegee intermediate

Criegee intermediate	Transition State Energy (kcal mol^{-1})	Imaginary Frequency (cm^{-1})	Product VHP	Product Energy (kcal mol^{-1})
syn-CH_3CHOO [a]	17.05	1696*i*	CH_2=CHOOH	-18.01
$(CH_3)_2COO$ [a]	16.16	1572*i*	CH_2=C(CH_3)OOH	-15.90
syn-CH_3CH_2CHOO [b]	16.46	1687*i*	*cis*-CH_3CH=CHOOH	-19.48
			trans-CH_3CH=CHOOH	-19.71
syn-trans-MVK-oxide [c]	17.96	1769.1*i*	*cis*-HPBD [d]	-12.02
syn-cis-MVK-oxide [c]	17.43	1763.5*i*	*trans*-HPBD [d]	-15.59

---

[a] Ref. [46]

[b] Ref. [56]

[c] MVK-oxide: methyl vinyl ketone oxide; (CH_2=CH)-(CH_3)COO; Ref. [62]

[d] HPBD:2-hydroperoxybuta-1,3-diene; (CH_2=CH)-(CH_2)-COOH

Figure 1: Reaction coordinate for *syn*-CH_3CHOO Criegee intermediate involving a rate-limiting 1,4-hydrogen transfer to vinyl hydroperoxide (VHP, $H_2C=CHOOH$) via a transition state (TS), followed by rapid decomposition to OH + vinoxy ($CH_2=CHO$) radical products.

Figure 2: Experimental rates (and corresponding lifetimes) for appearance of OH products following IR activation of *syn*-CH_3CHOO (red), $(CH_3)_2COO$ (light blue), CH_3CH_2CHOO (dark blue) , and MVK-oxide (cyan) Criegee intermediates over wide range of energies from 2000 cm^{-1} below to the vicinity of the theoretically predicted transition states (TS, vertical dashed lines) leading to OH products. Excellent agreement is obtained with RRKM rates (and corresponding lifetimes) with quantum mechanical tunneling (solid lines) for *syn*-CH_3CHOO and $(CH_3)_2COO$.
Data reproduced with permission of AIP publishing from Y. Fang et al., *J. Chem. Phys.* **144**, 061101 (2016); Y. Fang et al., *J. Chem. Phys.* **145**, 044312 (2016); Y. Fang et al., *J. Chem. Phys.* **145**, 234308 (2016); Y. Fang et al., *J. Chem. Phys* **146**, 134307 (2017). Data also reproduced with permission from V. P. Barber et al., *J. Am. Chem. Soc.* **140**, 10866–80 (2018). Copyright (2018) American Chemical Society.

Figure 3: Optimized structures and zero-point-corrected energies (kcal mol^{-1}) predicted for the four conformers of the MVK-oxide Criegee intermediate.
Reprinted with permission from V. P. Barber, S. Pandit, A. M. Green, N. Trongsiriwat, P. J. Walsh, S. R. Klippenstein, and M. I. Lester, "Four carbon Criegee intermediate from isoprene ozonolysis: Methyl vinyl ketone oxide synthesis, infrared spectrum, and OH production", *J. Am. Chem. Soc.* **140**, 10866–80 (2018). Copyright (2018) American Chemical Society.

Figure 4: Computed density of reactant states (solid lines; left axis) for the dimethyl- (light blue) and ethyl- (dark blue) substituted Criegee intermediates with the same mass and vibrational degrees of freedom, yet differing their torsional motions. By contrast, the tunneling weighted sum of states (dashed lines; right axis) at their respective transition states are remarkably similar with each containing a single methyl rotor.

Figure 5: Asymmetric one-dimensional Eckart potentials plotted in mass-weighted coordinates ($amu^{1/2}$ m) of the TS critical oscillator for isomerization of *syn*-CH_3CHOO (red), $(CH_3)_2COO$ (light blue), CH_3CH_2CHOO (dark blue), and MVK-oxide (cyan) Criegee intermediates to corresponding vinyl-substituted hydroperoxide species via 1,4-H-atom transfer. The curvature of the potential barrier at the TS is determined by the imaginary frequency. The zero-point corrected TS barrier heights in these systems differ by ca. 2 kcal mol^{-1}.

Figure 6: (Upper panel) RRKM calculation of microcanonical rate coefficient, k(E) (red), density of reactant states per cm^{-1}, N(E) (blue), and Boltzmann factor $\exp(-E/k_BT)$ at 300 K (black) for *syn*-CH_3CHOO. (Lower panel) The product of these three terms is plotted to illustrate their relative contributions at specific energies to the thermal rate coefficient k(T) at T = 260, 280, 300, and 320 K.
Reprinted from Y. Fang, F. Liu, V. P. Barber, S. J. Klippenstein, A. B. McCoy, and M. I. Lester, "Deep tunneling in the unimolecular decay of CH_3CHOO Criegee intermediates to OH

radical products", *J. Chem. Phys.* **145**, 234308 (2016), with the permission of AIP Publishing.

Figure 7: Arrhenius plot of the thermal decay rates k(T) predicted for *syn*-CH_3CHOO (red), $(CH_3)_2COO$ (light blue), CH_3CH_2CHOO (dark blue), and MVK-oxide (cyan) Criegee intermediates. The curvature in the temperature dependent thermal rates originates from quantum mechanical tunneling, which also significantly enhances the decay rates. Rates are computed using master equation modeling in the high-pressure limit, and are plotted as a function of inverse temperature from 200 to 370 K. (See Refs. 46, 55-57, 62 for additional details.)

Figure 8: Optimized structures and zero-point-corrected energies (kcal mol^{-1}) predicted for the four conformers of the MACR-oxide Criegee intermediate.
Reprinted with permission from M. F. Vansco, B. Marchetti, N. Trongsiriwat, G. Wang, T. Bhagde, P. J. Walsh, S. J. Klippenstein, and M. I. Lester, "Synthesis, electronic spectroscopy and photochemistry of methacrolein oxide: A four carbon unsaturated Criegee intermediate from isoprene ozonolysis", *J. Am. Chem. Soc.* **141**, 15058–69 (2019). Copyright 2019 American Chemical Society."

Figure 1

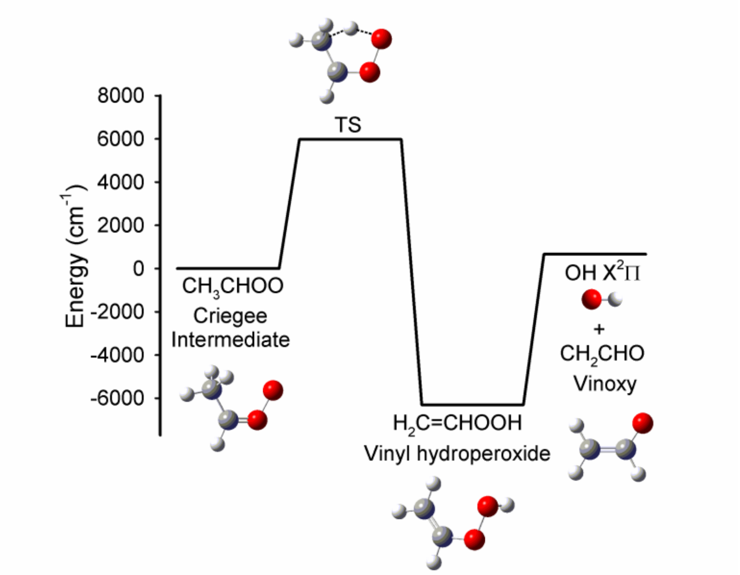

Figure 1: Reaction coordinate for *syn*-CH$_3$CHOO Criegee intermediate involving a rate-limiting 1,4-hydrogen transfer to vinyl hydroperoxide (VHP, H$_2$C=CHOOH) via a transition state (TS), followed by rapid decomposition to OH + vinoxy (CH$_2$=CHO) radical products.

Figure 2

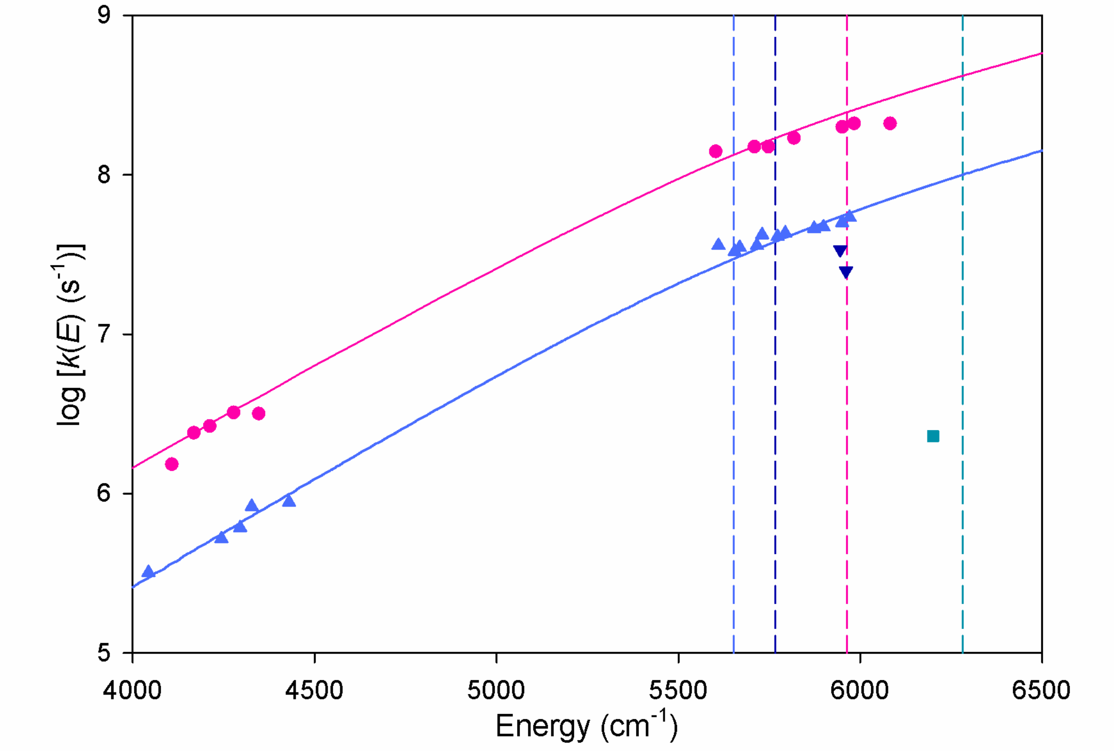

Figure 2: Experimental rates (and corresponding lifetimes) for appearance of OH products following IR activation of *syn*-CH_3CHOO (red), $(CH_3)_2COO$ (light blue), CH_3CH_2CHOO (dark blue) , and MVK-oxide (cyan) Criegee intermediates over wide range of energies from 2000 cm^{-1} below to the vicinity of the theoretically predicted transition states (TS, vertical dashed lines) leading to OH products. Excellent agreement is obtained with RRKM rates (and corresponding lifetimes) with quantum mechanical tunneling (solid lines) for *syn*-CH_3CHOO and $(CH_3)_2COO$.

Data reproduced with permission of AIP publishing from Y. Fang et al., *J. Chem. Phys.* **144**, 061101 (2016); Y. Fang et al., *J. Chem. Phys.* **145**, 044312 (2016); Y. Fang et al., *J. Chem. Phys.* **145**, 234308 (2016); Y. Fang et al., *J. Chem. Phys* **146**, 134307 (2017). Data also reproduced with permission from V. P. Barber et al., *J. Am. Chem. Soc.* **140**, 10866–80 (2018). Copyright (2018) American Chemical Society.

Figure 3

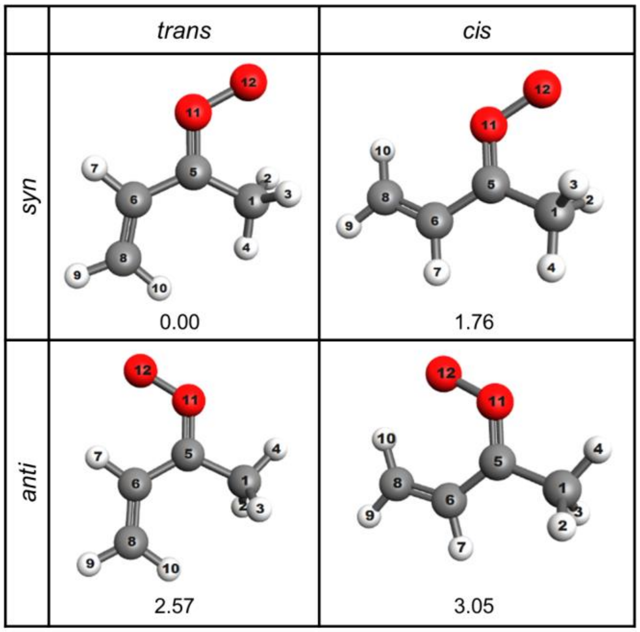

Figure 3: Optimized structures and zero-point-corrected energies (kcal mol^{-1}) predicted for the four conformers of the MVK-oxide Criegee intermediate.
Reprinted with permission from V. P. Barber, S. Pandit, A. M. Green, N. Trongsiriwat, P. J. Walsh, S. R. Klippenstein, and M. I. Lester, “Four carbon Criegee intermediate from isoprene ozonolysis: Methyl vinyl ketone oxide synthesis, infrared spectrum, and OH production”, *J. Am. Chem. Soc.* **140**, 10866–80 (2018). Copyright (2018) American Chemical Society.

Figure 4

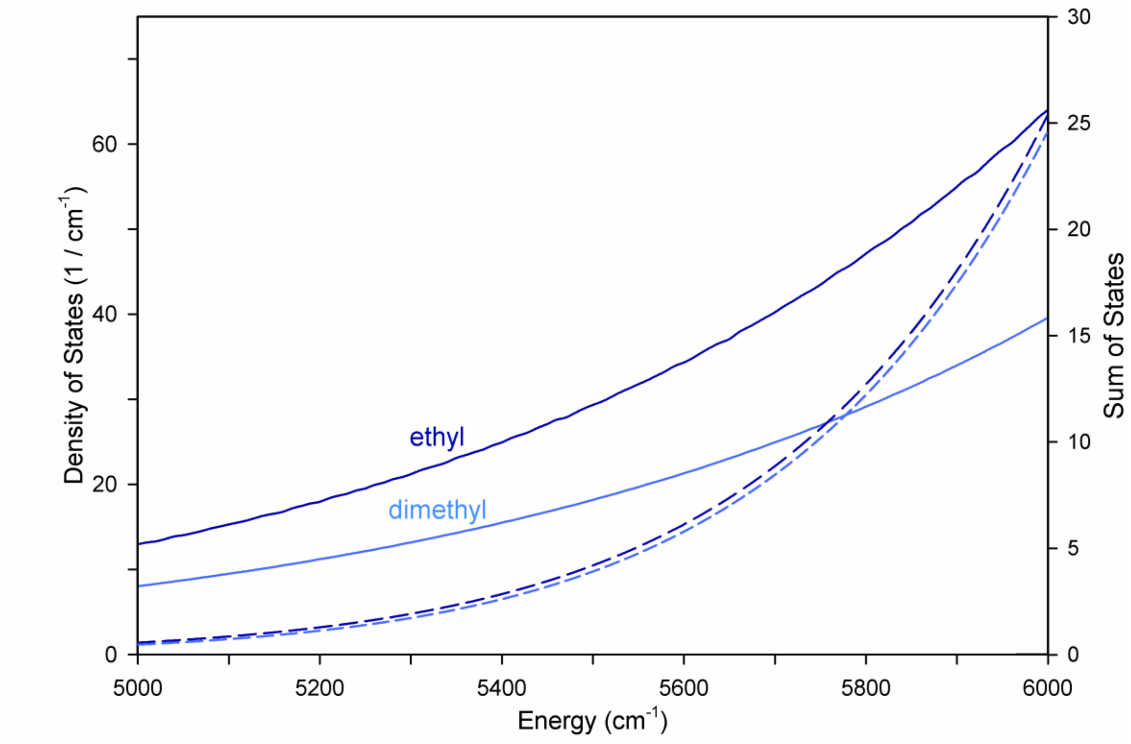

Figure 4: Computed density of reactant states (solid lines; left axis) for the dimethyl- (light blue) and ethyl- (dark blue) substituted Criegee intermediates with the same mass and vibrational degrees of freedom, yet differing their torsional motions. By contrast, the tunneling weighted sum of states (dashed lines; right axis) at their respective transition states are remarkably similar with each containing a single methyl rotor.

Figure 5

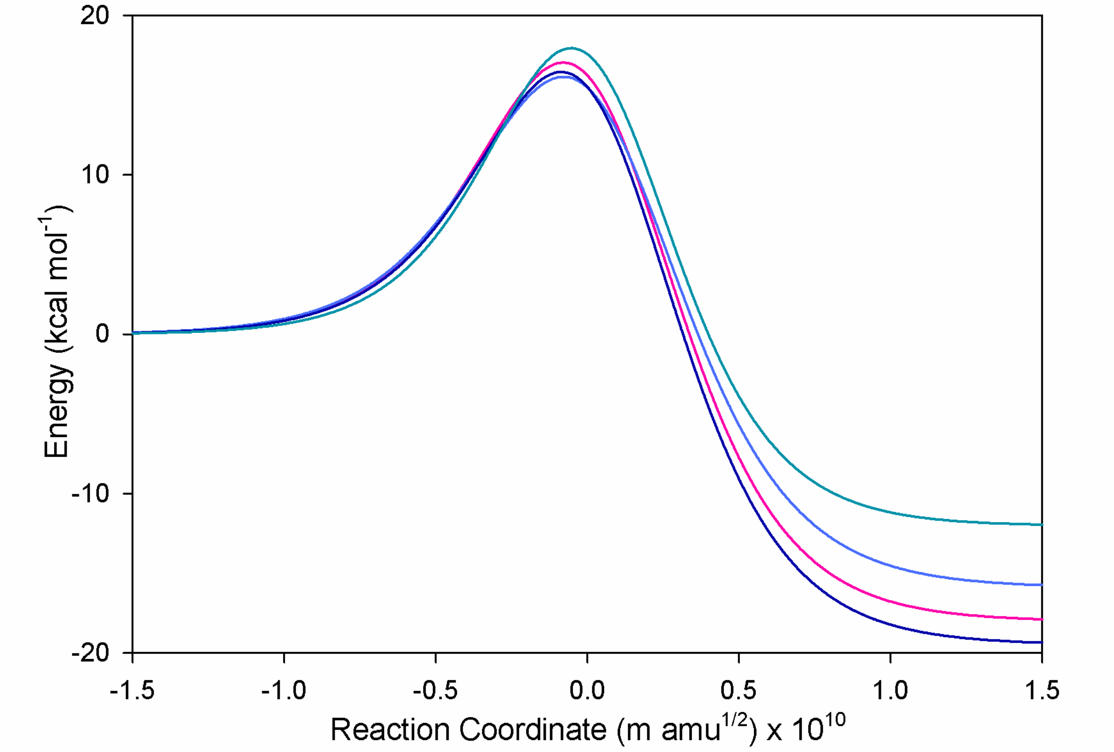

Figure 5: Asymmetric one-dimensional Eckart potentials plotted in mass-weighted coordinates (amu$^{1/2}$ m) of the TS critical oscillator for isomerization of *syn*-CH_3CHOO (red), $(CH_3)_2COO$ (light blue), CH_3CH_2CHOO (dark blue), and MVK-oxide (cyan) Criegee intermediates to corresponding vinyl-substituted hydroperoxide species via 1,4-H-atom transfer. The curvature of the potential barrier at the TS is determined by the imaginary frequency. The zero-point corrected TS barrier heights in these systems differ by ca. 2 kcal mol^{-1}.

Figure 6

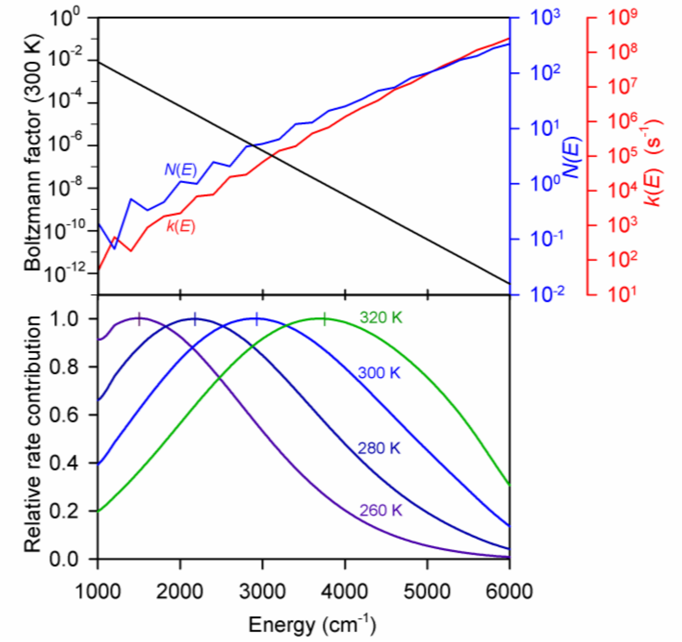

Figure 6: (Upper panel) RRKM calculation of microcanonical rate coefficient, k(E) (red), density of reactant states per cm^{-1}, N(E) (blue), and Boltzmann factor exp(-E/k_BT) at 300 K (black) for *syn*-CH_3CHOO. (Lower panel) The product of these three terms is plotted to illustrate their relative contributions at specific energies to the thermal rate coefficient k(T) at T = 260, 280, 300, and 320 K.

Reprinted from Y. Fang, F. Liu, V. P. Barber, S. J. Klippenstein, A. B. McCoy, and M. I. Lester, "Deep tunneling in the unimolecular decay of CH_3CHOO Criegee intermediates to OH radical products", *J. Chem. Phys.* **145**, 234308 (2016), with the permission of AIP Publishing.

Figure 7

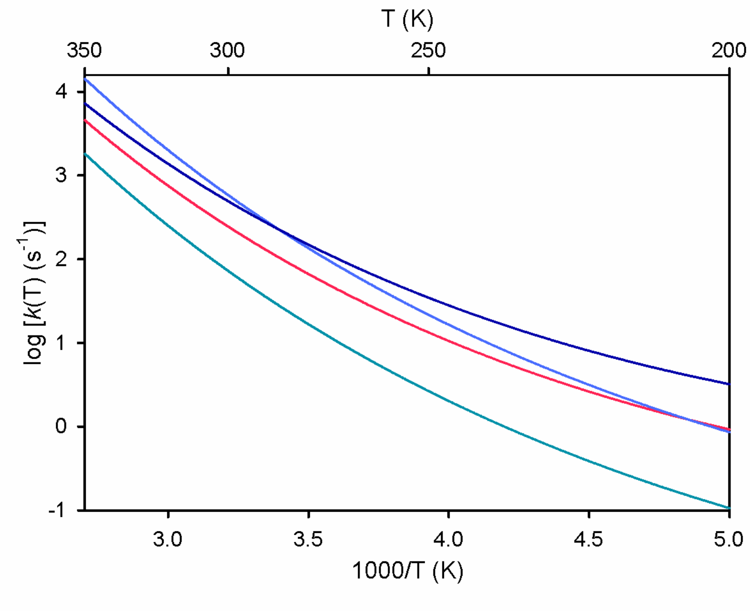

Figure 7: Arrhenius plot of the thermal decay rates k(T) predicted for *syn*-CH_3CHOO (red), $(CH_3)_2COO$ (light blue), CH_3CH_2CHOO (dark blue), and MVK-oxide (cyan) Criegee intermediates. The curvature in the temperature dependent thermal rates originates from quantum mechanical tunneling, which also significantly enhances the decay rates. Rates are computed using master equation modeling in the high-pressure limit, and are plotted as a function of inverse temperature from 200 to 370 K. (See Refs. 46, 55-57, 62 for additional details.)

Figure 8

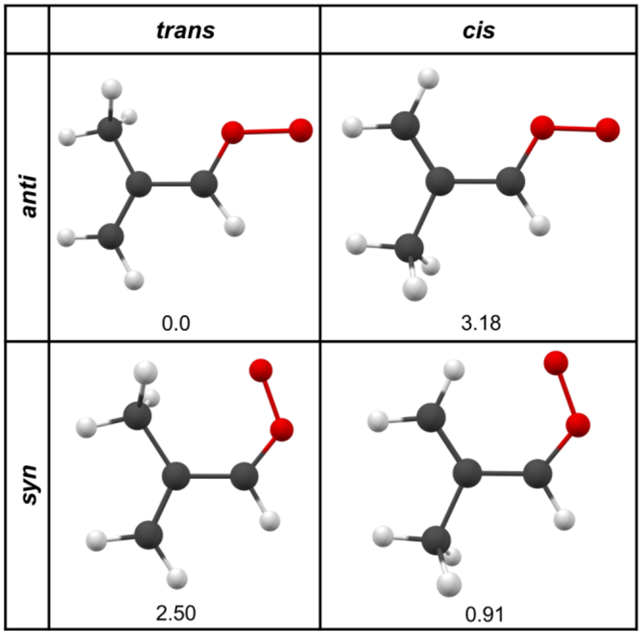

Figure 8: Optimized structures and zero-point-corrected energies (kcal mol^{-1}) predicted for the four conformers of the MACR-oxide Criegee intermediate.
Reprinted with permission from M. F. Vansco, B. Marchetti, N. Trongsiriwat, G. Wang, T. Bhagde, P. J. Walsh, S. J. Klippenstein, and M. I. Lester, “Synthesis, electronic spectroscopy and photochemistry of methacrolein oxide: A four carbon unsaturated Criegee intermediate from isoprene ozonolysis”, *J. Am. Chem. Soc.* **141**, 15058–69 (2019). Copyright 2019 American Chemical Society."